OPEN ACCESS
IOP Publishing
Journal of Physics A: Mathematical and Theoretical
J. Phys. A: Math. Theor. **58** (2025) 225202 (30pp)
https://doi.org/10.1088/1751-8121/adc95f

Non-linear sigma models for non-Hermitian random matrices in symmetry classes AI† and AII†

Anish Kulkarni[1,*], **Kohei Kawabata**[2] **and Shinsei Ryu**[1]

[1] Department of Physics, Princeton University, Princeton, NJ 08544, United States of America
[2] Institute for Solid State Physics, University of Tokyo, Kashiwa, Chiba 277-8581, Japan

E-mail: anishk@princeton.edu

Received 11 January 2025; revised 28 March 2025
Accepted for publication 4 April 2025
Published 27 May 2025

Abstract

Symmetry of non-Hermitian matrices underpins many physical phenomena. In particular, chaotic open quantum systems exhibit universal bulk spectral correlations classified on the basis of time-reversal symmetry† (TRS†), coinciding with those of non-Hermitian random matrices in the same symmetry class. Here, we analytically study the spectral correlations of non-Hermitian random matrices in the presence of TRS† with signs $+1$ and -1, corresponding to symmetry classes AI† and AII†, respectively. Using the fermionic replica non-linear sigma model approach, we derive n-fold integral expressions for the nth moment of the one-point and two-point characteristic polynomials, valid for any matrix dimension. We also study, in the limit of large matrix dimensions, the replica limit $n \to 0$ to derive the density of states and level–level correlations of non-Hermitian random matrices with TRS†. We compare our analytical findings with numerical results.

Keywords: random matrix theory, nonlinear sigma model, open quantum chaos, non-hermitian physics

* Author to whom any correspondence should be addressed.

1. Introduction

Random matrix theory (RMT), originally developed by Wigner to describe the energy levels of heavy atomic nuclei [1, 2], has since evolved into a versatile tool for understanding complex systems [3]. Its applications span numerous subfields of physics, including quantum chaos, Anderson localization, quantum chromodynamics , statistical mechanics, quantum information, and quantum gravity. Beyond physics, RMT has found widespread use in disciplines such as number theory, biological systems, and data science, among others. At its core, RMT studies the statistical properties of matrices with randomly chosen elements, providing insight into the behavior of large, interacting systems. In many cases, the eigenvalue distributions of these random matrices exhibit universal properties, meaning that they are largely independent of the specific details of the matrix ensemble. This universality is one of the most compelling features of RMT, making it applicable to diverse problems.

Non-Hermitian RMT extends the powerful framework of the traditional RMT to the study of matrices that lack Hermiticity [4]. While Hermitian matrices are central in quantum mechanics, non-Hermitian matrices emerge naturally in a wide array of physical systems where dissipation, gain, or non-conservative interactions play a role [5, 6]. These include open quantum systems, non-equilibrium statistical mechanics, disordered materials, and biological and sociological systems. The study of non-Hermitian random matrices began in earnest with the work of Ginibre [7], who introduced ensembles of non-Hermitian random matrices. Unlike Hermitian matrices, eigenvalues of non-Hermitian matrices generally spread over the complex plane, leading to rich and intricate spectral structures. One of the most remarkable features of non-Hermitian RMT is the emergence of complex spectral distributions, such as Girko's circular law [8], which describes the eigenvalue distribution for large non-Hermitian matrices with independent, identically distributed entries. Other classic works on non-Hermitian RMT are found, for example, in [9–15]. The relevance of non-Hermitian RMT has grown considerably in recent decades, particularly with the recognition of non-Hermitian physics in various fields. For example, beyond the Hermitian regime, the physics of Anderson localization in non-Hermitian systems has attracted growing interest [16–32]. Additionally, topological phenomena intrinsic to non-Hermitian systems have been extensively explored, offering new insights into the behavior of these systems [33, 34].

One of the key impacts of non-Hermiticity is the enrichment of symmetry classification, expanding the traditional 10-fold classification [35–38] to a more complex 38-fold scheme [39, 40]. This expanded classification is crucial not only for non-Hermitian RMT but also for understanding chaotic behavior in open quantum systems [41–69]. Similar to their Hermitian counterparts, spectral properties of non-Hermitian random matrices encode information about the dynamics of the associated physical system, many of which are expected to be universal. They are insensitive to the details of the ensemble distribution and classified based on the symmetry of the matrices in the ensemble.

For non-Hermitian matrices, time-reversal symmetry† (TRS†) plays a particularly important role [48]. It is defined by the relation $\mathcal{T}H\mathcal{T}^{-1} = H^\dagger$, where H is a non-Hermitian matrix and $\mathcal{T}$ is an anti-unitary operator. We distinguish two symmetry classes of non-Hermitian random matrices, AI† and AII† [40], which respect TRS† with $\mathcal{T}^2 = +1$ and $\mathcal{T}^2 = -1$, respectively. The presence of TRS† induces correlations among nearby complex eigenvalues. This should be contrasted with other discrete symmetries such as TRS, particle-hole symmetry (PHS) and PHS†—they relate complex eigenvalues with their complex-conjugate or opposite-sign partners. As a consequence, TRS† alters level statistics in the bulk of the complex spectrum, while TRS, PHS, and PHS† primarily affect spectral statistics around (near) symmetric lines or points. Moreover, just as the bulk spectral correlations of Hermitian random matrices in

symmetry classes A, AI, and AII are known to be universal, the bulk spectral correlations of non-Hermitian random matrices in symmetry classes A, AI†, and AII† are also expected to exhibit universal behavior. While numerical evidence supports this universality [48], a rigorous proof remains an open challenge. In this work, we take a step forward in this direction by analytically computing spectral correlations in the Gaussian ensemble for these symmetry classes. Figure 1 shows numerically calculated density of states and two-point correlation functions for classes A, AI† and AII†. The goal of our work is to develop analytical understanding of these quantities.

Non-linear σ models (NLσMs) have long been employed to calculate correlation functions in disordered systems [70]. Subsequently, field-theoretic treatments using the replica trick have been successfully used, even for non-Hermitian matrices. In [71], this method was used to calculate the density of states for non-Hermitian random matrices in classes A, AI, and AII. In this work, we further develop replica space NLσMs for classes AI† and AII†, which are relevant to the threefold universality classes of the bulk spectral correlations. Specifically, we consider the nth moments of the k-point characteristic polynomials $Z_n^{(k)}(z_1,\bar{z}_1,\ldots,z_k,\bar{z}_k)$, defined in equation (3), for Gaussian non-Hermitian random matrices in classes AI† and AII†. We also study the density of states, $R_1(z,\bar{z})$, and the two-point correlation function, $R_2(z_1,\bar{z}_1,z_2,\bar{z}_2)$, of the complex spectrum, derived from these polynomials via the replica limit $n\to 0$.

Our main results are summarized as follows. We derive general replica space matrix integrals for $Z_n^{(k)}(z_1,\bar{z}_1,\ldots,z_k,\bar{z}_k)$ in both symmetry classes AI† (equation (18)) and AII† (equation (68)). We then study the cases $k=1$ and $k=2$ in detail. For non-Hermitian random matrices of size N, we obtain exact expressions for $Z_n^{(1)}(z,\bar{z})$ with arbitrary N (equation (25) for class AI† and equation (73) for class AII†) and for $Z_n^{(2)}(z_1,\bar{z}_1,z_2,\bar{z}_2)$ in the limit $N\to\infty$ in both symmetry classes (equation (47) for class AI† and equation (90) for class AII†). These expressions are in the form of n-fold or $2n$-fold integrals over replica space singular values or cosine-sine values. We confirm these exact results by comparing them with numerically computed ensemble averages of characteristic polynomials. Furthermore, following the approach in [71–74], we perform the replica limit $n\to 0$ of these n-fold integrals to obtain closed form expressions for the spectral distributions $R_1(z,\bar{z})$ (equations (33) and (80)) and $R_2(z_1,\bar{z}_1,z_2,\bar{z}_2)$ (equations (56) and (99)) in the regimes $|z|\ll\sqrt{N}$ and $|z_1-z_2|\ll\sqrt{N}$, respectively. We compare our analytical findings and numerical results. For the density of states, our results show reasonable agreement with the numerics within the range of their validity. However, for the two-point function, our results substantially deviate from the numerics in the regime $|z_1-z_2|\lesssim\sqrt{g}$ where level repulsion among complex eigenvalues is prominent. To obtain more accurate results, refining our current approach or adopting a more systematic method for taking the replica limit may be necessary.

2. NLσM for class AI†

2.1. Replica space matrix integral for characteristic polynomials

Non-Hermitian matrices in class AI† are defined to respect TRS† with sign $+1$:

$$H^\dagger=\mathcal{T}H\mathcal{T}^{-1}=\bar{H}, \tag{1}$$

where we choose the symmetry operator $\mathcal{T}$ to be complex conjugation $\mathcal{K}$, and $\bar{H}$ denotes complex conjugate of H. This is equivalent to $H=H^T$, where H^T denotes the transpose of H. We

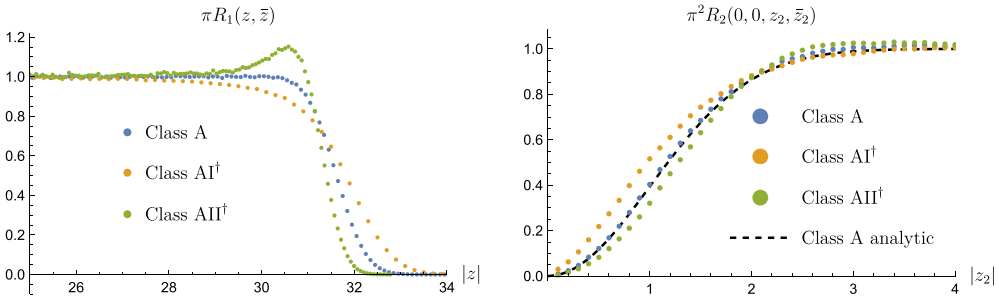

Figure 1. Numerical calculations for one-point (left) and two-point (right) functions for the three universality classes. We sample matrices of size $10^3 \times 10^3$ for classes A and AI† and size $\left(2 \times 10^3\right) \times \left(2 \times 10^3\right)$ for class AII†. To numerically obtain R_1, we simply compute the histogram of the sampled spectra in each class. The numerical computation of R_2 is more subtle. To analyze bulk correlations, we must choose eigenvalues away from the edge of the spectrum. Our prescription is to choose eigenvalues within a disc centered at the origin with $2/3^{\text{rd}}$ the radius of the spectrum. In this region, R_2 depends only on the distance $|z_1 - z_2|$. Therefore, the Mathematica library function `PairCorrelationG` can be used, which gives $\rho^{-2} R_2(\sqrt{\rho}|z_1 - z_2|)$, where ρ is the density of eigenvalues in this region. We then average this quantity over 10^3 samples in each class. In the above plot, to compare correlations across different classes, we have scaled the data such that ρ is identical for each class. For comparison, we also plot the known analytical result for the bulk two-point correlation function in class A [75].

thus consider a Gaussian ensemble of symmetric $N \times N$ complex matrices H:

$$\begin{aligned} P(H)\,\mathrm{d}H &= \mathrm{d}H \exp\left[-g^{-1}\,\mathrm{tr}\,H^\dagger H\right] \\ &= \mathcal{N}_{\mathrm{AI}^\dagger} \prod_{i=1}^{N} \mathrm{d}H_{ii}\mathrm{d}H_{ii}^* \prod_{1\leqslant i<j\leqslant N} \mathrm{d}H_{ij}\mathrm{d}H_{ij}^* \exp\left[-g^{-1}\left(\sum_{i=1}^{N}|H_{ii}|^2 + 2\sum_{1\leqslant i<j\leqslant N}|H_{ij}|^2\right)\right] \end{aligned} \tag{2}$$

where g parameterizes the width of the Gaussian and the normalization $\mathcal{N}_{\mathrm{AI}^\dagger}$ is defined by setting $\int \mathrm{d}H P(H) = 1$. Our main objects of interest are the nth moments of kth-order characteristic polynomial of H, defined as

$$Z_n^{(k)}(z_1,\bar{z}_1,\ldots,z_k,\bar{z}_k) = \left\langle \prod_{l=1}^{k} \det(z_l - H)^n \det\left(\bar{z}_l - H^\dagger\right)^n \right\rangle, \tag{3}$$

where the angular brackets represent the ensemble averaging with respect to the probability measure in equation (2), $\langle\cdots\rangle = \int \mathrm{d}H P(H)\cdots$. Following the replica trick, the k-point correlation functions of complex eigenvalues of H can be determined using $Z_n^{(k)}(z_1,\bar{z}_1,\ldots,z_k,\bar{z}_k)$ (see [71, 76] for details). For simplicity, we will first derive the replica space matrix integral for $k = 1$. A few modifications will give the auxiliary field matrix integral for general k.

The determinants are re-expressed as Grassmann integrals,

$$\begin{aligned} Z_n^{(1)}(z,\bar{z}) = &\int \mathrm{d}H P(H) \int \mathrm{d}\psi\,\mathrm{d}\bar{\psi} \exp\left[-\bar{\psi}_a^i\left(z\delta^{ij}\delta^{ab} - H^{ij}\delta^{ab}\right)\psi_a^j\right] \\ &\times \int \mathrm{d}\chi\,\mathrm{d}\bar{\chi} \exp\left[-\bar{\chi}_a^i\left(\bar{z}\delta^{ij}\delta^{ab} - \left(H^\dagger\right)^{ij}\delta^{ab}\right)\chi_a^j\right], \end{aligned} \tag{4}$$

where $\psi_a^i, \bar{\psi}_a^i, \chi_a^i, \bar{\chi}_a^i$ are independent Grassmann variables. They satisfy the anti-commutation relation $\{\eta, \xi\} = 0$, where η, ξ are any of $\psi_a^i, \bar{\psi}_a^i, \chi_a^i, \bar{\chi}_a^i$. In equation (4) and from now on, we use the convention for implicitly summing repeated indices. For Grassmann integrals, we use conventions from [70]. The indices $i,j = 1,\ldots,N$ are color/matrix indices, and $a,b = 1,\ldots,n$ are flavor/replica indices. Since H is symmetric, it is only coupled with the symmetric part of the fermion bilinears $\left\lfloor \psi_a \bar{\psi}_a^T \right\rfloor = \frac{1}{2}\left(\psi_a \bar{\psi}_a^T - \bar{\psi}_a \psi_a^T\right)$. Specifically, we have

$$\bar{\psi}_a^i H^{ij} \psi_a^j = -\mathrm{tr}\left(H \left\lfloor \psi_a \bar{\psi}_a^T \right\rfloor\right). \tag{5}$$

The Gaussian integral over H gives a quartic action for the fermions,

$$Z_n^{(1)}(z,\bar{z}) = \int \mathrm{d}\psi\, \mathrm{d}\bar{\psi}\, \mathrm{d}\chi\, \mathrm{d}\bar{\chi}\; e^{S[\psi,\chi]}, \tag{6}$$

$$S[\psi,\chi] = \bar{z}\mathrm{tr}\left(\left\lfloor \chi_a \bar{\chi}_a^T \right\rfloor\right) + z\mathrm{tr}\left(\left\lfloor \psi_a \bar{\psi}_a^T \right\rfloor\right) + g\mathrm{tr}\left(\left\lfloor \chi_a \bar{\chi}_a^T \right\rfloor \left\lfloor \psi_b \bar{\psi}_b^T \right\rfloor\right). \tag{7}$$

The quartic term above is expressed in terms of color-space matrices. We rearrange it as follows to express it in terms of flavor/replica space matrices,

$$\mathrm{tr}\left(\left\lfloor \chi_a \bar{\chi}_a^T \right\rfloor \left\lfloor \psi_b \bar{\psi}_b^T \right\rfloor\right) = \frac{1}{2}\left(\left(\psi_b^T \chi_a\right)\left(\bar{\chi}_a^T \bar{\psi}_b\right) - \left(\bar{\psi}_b^T \chi_a\right)\left(\bar{\chi}_a^T \psi_b\right)\right). \tag{8}$$

Now, we introduce replica space auxiliary fields to decouple these quartic terms into quadratic terms using the Hubbard–Stratonovich transformations. We use 'Tr' for the trace in flavor space. We introduce flavor space matrices Q and $R \in \mathbb{C}^{n\times n}$ to decouple, respectively, the first and second terms of equation (8),

$$\exp\left[-\frac{1}{2}g\mathrm{Tr}\left(\left(\bar{\psi}^T\chi\right)\left(\bar{\chi}^T\psi\right)\right)\right] \propto \int \mathrm{d}Q \exp\left[-\frac{1}{2}g^{-1}\mathrm{Tr}\left(QQ^\dagger\right) - \frac{1}{2}\mathrm{Tr}\left(\bar{\psi}^T\chi Q^\dagger\right) + \frac{1}{2}\mathrm{Tr}\left(Q\bar{\chi}^T\psi\right)\right]. \tag{9}$$

Similarly, we have

$$\exp\left[\frac{1}{2}g\mathrm{Tr}\left(\left(\psi^T\chi\right)\left(\bar{\chi}^T\bar{\psi}\right)\right)\right] \propto \int \mathrm{d}R \exp\left[-\frac{1}{2}g^{-1}\mathrm{Tr}\left(RR^\dagger\right) - \frac{1}{2}\mathrm{Tr}\left(R^\dagger\psi^T\chi\right) - \frac{1}{2}\mathrm{Tr}\left(\bar{\chi}^T\bar{\psi}R\right)\right]. \tag{10}$$

If we collect all Grassmann variables into one vector

$$\Psi^i = \left(\psi_1^i,\ldots,\psi_n^i,\chi_1^i,\ldots,\chi_n^i,\bar{\psi}_1^i,\ldots,\bar{\psi}_n^i,\bar{\chi}_1^i,\ldots,\bar{\chi}_n^i\right)^T, \tag{11}$$

and define the $4n \times 4n$ matrix

$$\mathbf{M} = \frac{1}{2}\begin{pmatrix} 0 & \bar{R} & -2z\mathbb{I}_n & Q \\ -R^\dagger & 0 & -Q^\dagger & -2\bar{z}\mathbb{I}_n \\ 2z\mathbb{I}_n & \bar{Q} & 0 & -R \\ -Q^T & 2\bar{z}\mathbb{I}_n & R^T & 0 \end{pmatrix}, \tag{12}$$

then the resulting action has the quadratic form, $S = -\frac{1}{2}\Psi^{iT}\mathbf{M}\Psi^i$. The matrix $\mathbf{M}$ is an antisymmetric matrix. The integral over the Grassmann fields can now be performed, which gives the Pfaffian of $\mathbf{M}$:

$$Z_n^{(1)}(z,\bar{z}) = \int_{\mathbb{C}^{n\times n}} \mathrm{d}Q \int_{\mathbb{C}^{n\times n}} \mathrm{d}R \exp\left[-\frac{1}{2}g^{-1}\mathrm{tr}\left(Q^\dagger Q + R^\dagger R\right)\right] \det{}^{\frac{N}{2}}\mathbf{M}. \tag{13}$$

By a basis change, $\det \mathbf{M}$ can be rewritten as the determinant of the following $2n \times 2n$ matrix:

$$\frac{1}{2}\begin{pmatrix} 2\bar{z}\mathbb{I}_n & 0 & R^T & -Q^T \\ 0 & 2\bar{z}\mathbb{I}_n & Q^\dagger & R^\dagger \\ -\bar{R} & -Q & 2z\mathbb{I}_n & 0 \\ \bar{Q} & -R & 0 & 2z\mathbb{I}_n \end{pmatrix} = \begin{pmatrix} \bar{z}\mathbb{I}_n & \mathcal{Q} \\ -\mathcal{Q}^\dagger & z\mathbb{I}_n \end{pmatrix}, \quad \mathcal{Q} = \frac{1}{2}\begin{pmatrix} R^T & -Q^T \\ Q^\dagger & R^\dagger \end{pmatrix}. \tag{14}$$

The matrix $\mathcal{Q}$ satisfies

$$\Sigma_n^y \mathcal{Q} = \bar{\mathcal{Q}}\Sigma_n^y, \quad \Sigma_n^y = \sigma^y \otimes \mathbb{I}_n = \begin{pmatrix} 0 & -i\mathbb{I}_n \\ i\mathbb{I}_n & 0 \end{pmatrix}. \tag{15}$$

By noticing $\mathrm{tr}(\mathcal{Q}^\dagger \mathcal{Q}) = (1/2)\mathrm{tr}(QQ^\dagger + RR^\dagger)$, the characteristic polynomial is expressed as

$$Z_n^{(1)}(z,\bar{z}) = \int_{\mathcal{M}} \mathrm{d}\mathcal{Q}\, \mathrm{e}^{-g^{-1}\mathrm{tr}\mathcal{Q}^\dagger\mathcal{Q}} \det{}^{N/2} \begin{pmatrix} \bar{z}\mathbb{I}_n & \mathcal{Q} \\ -\mathcal{Q}^\dagger & z\mathbb{I}_n \end{pmatrix}, \tag{16}$$

with

$$\mathcal{M} = \left\{ \mathcal{Q} \in \mathbb{C}^{2n\times 2n} \mid \Sigma_n^y \mathcal{Q} = \bar{\mathcal{Q}}\Sigma_n^y \right\}. \tag{17}$$

Now, we generalize this expression to the k-point characteristic polynomial. A straightforward extension of the above procedure gives the same expressions as above, with $z\mathbb{I}_n$ and Σ_n^y replaced by matrices Z and Σ_{nk}^y, defined momentarily. Using a suitable (orthogonal) similarity transformation on Q, Z, and Σ_{nk}^y, we can choose $Z = \mathrm{diag}(z_1, \ldots, z_k) \otimes \mathbb{I}_{2n}$ and $\Sigma_{nk}^y = \sigma^y \otimes \mathbb{I}_{nk}$ without loss of generality. The characteristic polynomial for the k-point function is then given as

$$Z_n^{(k)}(z_1, \bar{z}_1, \ldots, z_k, \bar{z}_k) = \int_{\mathcal{M}} \mathrm{d}\mathcal{Q}\, \mathrm{e}^{-g^{-1}\mathrm{tr}\mathcal{Q}^\dagger\mathcal{Q}} \det{}^{N/2} \begin{pmatrix} \bar{Z} & \mathcal{Q} \\ -\mathcal{Q}^\dagger & Z \end{pmatrix}, \tag{18}$$

with

$$\mathcal{M} = \left\{ \mathcal{Q} \in \mathbb{C}^{2nk\times 2nk} \mid \Sigma_{nk}^y \mathcal{Q} = \bar{\mathcal{Q}}\Sigma_{nk}^y \right\}. \tag{19}$$

In the subsequent sections, we will compute this integral for $k = 1$ and $k = 2$ under suitable limits.

2.2. One-point characteristic polynomial

The integral expression in equation (16), playing a role of the partition function, can be further evaluated in various ways. Let us first discuss the behavior in the large-N limit. In the limit $N \to \infty$, we can use the saddle-point approximation to calculate $Z_n^{(1)}(z,\bar{z})$. The saddle-point equation for the action in equation (16) is

$$\mathcal{Q}^\dagger \mathcal{Q} = \left(\frac{gN}{2} - |z|^2 \right) \mathbb{I}_{2n}. \tag{20}$$

For $|z|^2 < gN/2$, the solution is simply

$$\mathcal{Q} = \sqrt{\frac{gN}{2} - |z|^2}\, U, \tag{21}$$

where U is a unitary matrix that satisfies $\Sigma_n^y U = \bar{U}\Sigma_n^y$ (or equivalently, $U\Sigma_n^y U^T = \Sigma_n^y$), i.e. $U \in \mathrm{Sp}(n)$. Now, we substitute this solution into equation (16) and obtain the dominant contribution at large N, leading to

$$\begin{aligned} Z_n^{(1)}(z,\bar{z}) &\simeq \int_{\mathrm{Sp}(n)} \mathrm{d}U\, \mathrm{e}^{\left(g^{-1}|z|^2 - \frac{N}{2}\right)\mathrm{tr}\mathbb{I}_{2n}}\, \det{}^{N/2}\left(g\frac{N}{2}\mathbb{I}_{2n}\right) \\ &= \mathrm{e}^{2ng^{-1}|z|^2}\left[\mathrm{e}^{-nN}\left(\frac{gN}{2}\right)^{nN}\mathrm{Vol}\left(\mathrm{Sp}(n)\right)\right]. \end{aligned} \tag{22}$$

Note that the factors inside the square bracket drop out in the replica limit $n \to 0$. In the next subsection, we will use this expression to discuss the density of states.

Now, let us go back to equation (16) and evaluate it without the large-N approximation. We consider the singular-value decomposition of $\mathcal{Q}$,

$$\mathcal{Q} = U\Lambda V; \quad V \in \mathrm{Sp}(n),\ U \in \mathrm{Sp}(n)/\mathrm{Sp}(1)^{\oplus n}, \quad \Lambda = \mathrm{diag}\left(\lambda_1^{\frac{1}{2}},\ldots,\lambda_n^{\frac{1}{2}},\lambda_1^{\frac{1}{2}},\ldots,\lambda_n^{\frac{1}{2}}\right) \quad (\lambda_a \geqslant 0). \tag{23}$$

To find the measure in terms of U, Λ, and V, we must calculate the determinant of the Jacobian $\frac{\partial \mathcal{Q}}{\partial[U,\Lambda,V]}$ for this transformation. See appendix B and [77] for more details. The measure is given as

$$\mathrm{d}\mathcal{Q} = \mathrm{d}U\mathrm{d}V|\Delta(\lambda)|^4 \prod_{a=1}^{n} \mathrm{d}\lambda_a\, \lambda_a, \quad \Delta(\lambda) = \prod_{a>b}^{n}(\lambda_a - \lambda_b). \tag{24}$$

Here, $\mathrm{d}U$ and $\mathrm{d}V$ represent the Haar measure on $\mathrm{Sp}(n)$, the integral over which is just an overall constant and is irrelevant in the replica limit. The only relevant degrees of freedom in the replica space are λ_a, and hence we have

$$Z_n^{(1)}(z,\bar{z}) \simeq \int_0^{\infty} \prod_{a=1}^{n} \mathrm{d}\lambda_a\, \mathrm{e}^{-2g^{-1}\lambda_a}\left(|z|^2 + \lambda_a\right)^N \lambda_a |\Delta(\lambda)|^4. \tag{25}$$

We highlight that this is an exact expression for all moments of the one-point characteristic polynomial at arbitrary N and z, up to an overall constant. This can also be thought of as a partition function for replica space degrees of freedom λ_a. We note that there exist other results on this quantity in [78, 79]. We also note that there exists another work [80] which studies similar objects.

In figure 2, we plot the analytical expression in equation (25) of the characteristic polynomial for various values of N and n as a function of $|z|$. We also compare the analytical result in equation (2) with numerical results where we numerically generate non-Hermitian random matrices from the Gaussian ensemble in equation (2) and calculate the characteristic polynomial. For all values of N and n we studied, we have a good agreement between the analytical and numerical results. While figure 2 shows a good agreement of the derived formula in equation (25) and the numerics, it should be noted that, in the interest of the universal statistics of non-Hermitian random matrix theory, it is known that the small N behaviour is not a good approximation for the large N limit. This fact was pointed out for class A in [41] and was also further studied for the $N = 2$ behaviour of classes AI† and AII† in [81].

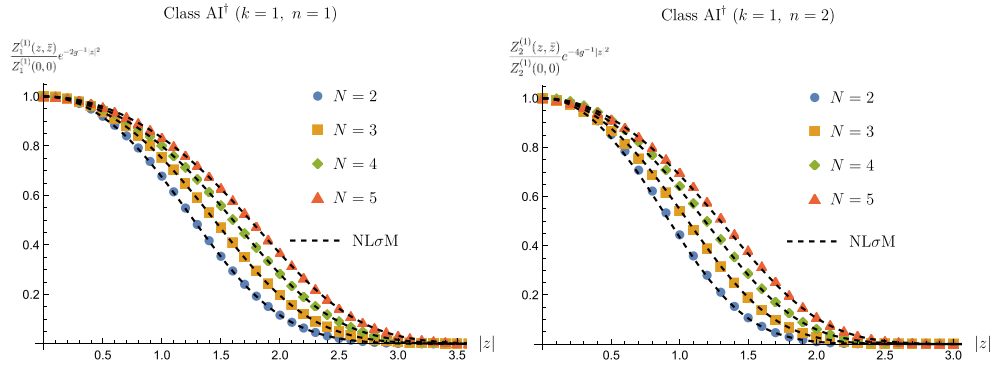

Figure 2. Plot of $\frac{Z_n^{(1)}(z,\bar{z})}{Z_n^{(1)}(0,0)}\mathrm{e}^{-2ng^{-1}|z|^2}$ as a function of $|z|$ for class AI†. For each value of N, we sample 10^5 non-Hermitian random matrices according to equation (2) with $g=2$. The solid markers show the ensemble-averaged characteristic polynomials. The black dashed curves show the same quantity calculated by the NLσM in equation (25).

2.2.1. Density of states. The density of states, $R_1(z,\bar{z})$, is determined from the first-order characteristic polynomial by [71, 76]

$$\pi R_1(z,\bar{z}) = \lim_{n\to 0}\frac{1}{n}\partial_{\bar{z}}\partial_z Z_n^{(1)}(z,\bar{z}). \tag{26}$$

To begin with, we extract the dominant contribution to $R_1(z,\bar{z})$ at large N. We expect this contribution to be a uniform distribution on a disk centered at the spectral origin, which is verified from the NLσM as follows. In the large N limit, using equations (22) and (26), we obtain

$$\pi R_1(z,\bar{z}) = \lim_{n\to 0}\frac{1}{n}\partial_{\bar{z}}\partial_z Z_n^{(1)}(z,\bar{z}) = \frac{2}{g} \quad \text{for} \quad |z|^2 < \frac{gN}{2}. \tag{27}$$

Indeed, at large N, the density of states is a uniform distribution on a disc of radius $\sqrt{gN/2}$ centered at the origin, which is consistent with Girko's circular law [8].

To discuss the density of states near the edge of the spectrum, we use equation (25) and analyze its behavior at large N and in the limit $n\to 0$. For large N, we can further perform a saddle-point approximation. We set $g=2$ for simplicity and consider the factor $I(\lambda) = e^{-\lambda_a}\left(|z|^2+\lambda_a\right)^N$ in the integrand. For large N, $I(\lambda)$ approaches an un-normalized Gaussian. The saddle point obtained by solving $\partial_\lambda \ln(I(\lambda)) = 0$ is $\lambda_{\rm sp} = N - |z|^2$. We Taylor-expand the action around this saddle point, $\ln I(\lambda) \sim -\lambda_{\rm sp} + N\ln N - \frac{(\lambda-\lambda_{\rm sp})^2}{2N}$, and substitute this back into equation (25). Rescaling $\lambda \to \lambda_{\rm sp}\lambda$ and ignoring irrelevant overall factors, we obtain

$$Z_n^{(1)}(z,\bar{z}) \simeq \mathrm{e}^{-n\lambda_{\rm sp}}\lambda_{\rm sp}^{2n^2}\int_0^\infty \prod_{a=1}^{n}\mathrm{d}\lambda_a\, \exp\left(-\frac{\lambda_{\rm sp}^2}{2N}(\lambda_a-1)^2\right)|\lambda_a||\Delta(\lambda)|^4. \tag{28}$$

Now, we rewrite the contour of integration as a sum over two contours: $\int_0^\infty \mathrm{d}\lambda \to \int_{-\infty}^\infty \mathrm{d}\lambda - \int_{-\infty}^0 \mathrm{d}\lambda$ for each λ. This gives us

$$Z_n^{(1)}(z,\bar{z}) \simeq \mathrm{e}^{-n\lambda_{\mathrm{sp}}} \lambda_{\mathrm{sp}}^{2n^2} \sum_p (-1)^p \binom{n}{p} \int_{-\infty}^0 \prod_{a=1}^p \mathrm{d}x_a \exp\left(-\frac{\lambda_{\mathrm{sp}}^2}{2N}(x_a-1)^2\right) |x_a| |\Delta(x)|^4 \times \int_{-\infty}^\infty \prod_{a=1}^{n-p} \mathrm{d}y_a \exp\left(-\frac{\lambda_{\mathrm{sp}}^2}{2N}(y_a-1)^2\right) |y_a| |\Delta(y)|^4. \tag{29}$$

We have considered the regime where $\lambda_{\mathrm{sp}}^2/2N$ is large enough so that x and y accumulate near the maxima of the weight function, i.e. 0 and 1. As such, we can approximate $\Delta(\lambda) \simeq \Delta(x)\Delta(y)$, and the x and y variables become decoupled. In the y-integral, since the Gaussian is narrowly peaked at 1, we replace the factor of y_a in the integrand with 1. The remaining integral is then a Selberg integral that is evaluated exactly,

$$\int_{-\infty}^\infty \prod_{a=1}^{n-p} \mathrm{d}y_a \exp\left(-\frac{\lambda_{\mathrm{sp}}^2}{2N}(y_a-1)^2\right) |\Delta(y)|^4 \simeq \left(\frac{\lambda_{\mathrm{sp}}}{\sqrt{N}}\right)^{-2(n-p)^2+(n-p)} \left(\frac{2}{\pi}\right)^{p/2} \prod_{a=1}^{n-p} \Gamma(1+2a). \tag{30}$$

Before proceeding to the x-integral, we should look at the coefficient of the pth term in this expansion and identify which terms survive in the replica limit $n \to 0$. The coefficient is $\binom{n}{p} \prod_{a=1}^{n-p} \Gamma(1+2a)$. At order n, the coefficient is 1 and n for $p=0$ and 1, respectively, and vanishes for all $p \geqslant 2$. We then have

$$\int_{-\infty}^0 \mathrm{d}x_1 \exp\left(-\frac{\lambda_{\mathrm{sp}}^2}{2N}(x_1-1)^2\right) |x_1| \simeq \frac{N^2}{\lambda_{\mathrm{sp}}^4} \exp\left(-\frac{\lambda_{\mathrm{sp}}^2}{2N}\right) \quad \text{for} \quad \frac{\lambda_{\mathrm{sp}}^2}{2N} \gg 1. \tag{31}$$

Putting it all together, we have

$$Z_n^{(1)}(z,\bar{z}) \simeq 1 - n\lambda_{\mathrm{sp}} + n\ln\lambda_{\mathrm{sp}} - n\left(\frac{2}{\pi}\right)^{1/2} \left(\frac{\lambda_{\mathrm{sp}}}{\sqrt{N}}\right)^{-7} \exp\left(-\frac{\lambda_{\mathrm{sp}}^2}{2N}\right) + \mathcal{O}(n^2). \tag{32}$$

Finally, plugging this into equation (26) and keeping the leading-order terms lead to

$$\pi R_1(z,\bar{z}) = 1 - \frac{1}{4u^2} - \sqrt{\frac{2}{\pi N}} \frac{\mathrm{e}^{-2u^2}}{16u^4} - \frac{\mathrm{e}^{-2u^2}}{16\sqrt{2\pi}\,u^5}, \tag{33}$$

where we introduce $u = \sqrt{N} - |z|$ as the distance of z from the edge of the spectrum, and use $\lambda_{\mathrm{sp}} \simeq 2u\sqrt{N}$. We expect that the fermionic replica method can only reproduce the tail of the density of states for $|z| < \sqrt{gN/2}$ [71]. Furthermore, note that we assumed $|z| \ll \sqrt{gN/2}$ in our approximations. In the above analysis and in equation (33), the g dependence can be added back using dimensional analysis.

In figure 3, we compare the analytical result from equation (33) with the density of states obtained from numerical calculations for $g=2$ and $N=10^3$. Note that figure 3 is a logarithmic plot for the difference $\pi(R_1(0,0) - R_1(z,\bar{z}))$, which may visually amplify the spread of the numerical data. Additionally, equation (33) is strictly valid only for $|z| \ll \sqrt{gN}/2 \approx 31.6$ given the choice of parameters in figure 3. Within these limitations, the NLσM result and the numerical calculations appear consistent for $22 \lesssim |z| \lesssim 30$. For $|z| \gtrsim 30$, equation (33) begins

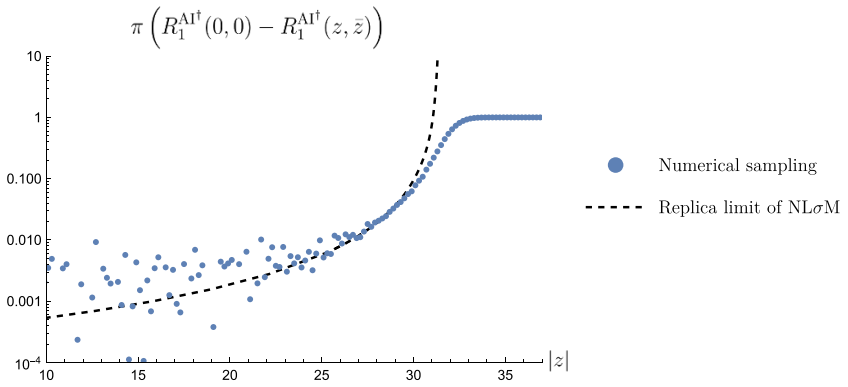

Figure 3. Comparison between the analytical result in equation (33) and the density of states obtained from numerical calculations. The numerical results are obtained using 2×10^4 realizations of $10^3 \times 10^3$ non-Hermitian random matrices in class $\mathrm{AI}^\dagger$ sampled according to equation (2) with $g = 2$. Note that this is a logarithmic plot. This might cause the spread of the numerics in the plot.

to deviate from the numerical results. For $|z| \lesssim 20$, the analytical result and the numerical data are consistent within $\sim 10^{-2}$, although the numerical data scatter due to the logarithmic plot. A more precise comparison with large-scale numerics, along with an analysis that includes corrections beyond the saddle-point approximation, is left for future study. Furthermore, while our approach of taking the replica limit is inspired by [72–74], there remains room for improvement on these calculations. For example, in the standard case of the Gaussian unitary ensemble in Hermitian RMT, the replica limit can be taken more systematically once we know the recursion relation satisfied by the replica partition functions with different replica indices, and also the partition functions with negative replica indices, which can be obtained from bosonic replica NLσM [72–74, 82–85]. In the context of non-Hermitian random matrices, these issues were discussed in detail for the Ginibre unitary ensemble in [86]. Additionally, it should be useful to develop a supersymmetric NLσM approach.

2.3. *Two-point characteristic polynomial*

We now discuss the second-order characteristic polynomial, $Z_n^{(2)}$, starting from equation (18). For large N, the integral over $\mathcal{Q}$ can be approximated by an integral over the saddle-point manifold. We introduce the radius of the spectrum, $r_\mathrm{s} = \sqrt{gN/2}$, and focus on the region in the bulk of the spectrum, $|z_{1,2}| \ll r_\mathrm{s}$, where the saddle-point equation is simplified to

$$\mathcal{Q}^\dagger \mathcal{Q} = r_\mathrm{s}^2 \, \mathbb{I}_{4n}. \tag{34}$$

The solution is $\mathcal{Q} = r_\mathrm{s} U$, with a unitary matrix U. Moreover, owing to $\mathcal{Q} \in \mathcal{M}$ (see equation (19)), we have

$$U \Sigma^y_{nk} U^T = \Sigma^y_{nk} \bar{U} U^T = \Sigma^y_{nk}. \tag{35}$$

Thus, U is symplectic and unitary, and thus belongs to the symplectic group $\mathrm{Sp}(2n)$. We substitute the saddle-point solution back into the expression for $Z_n^{(2)}(z_1,\bar{z}_1,z_2,\bar{z}_2)$, leading to

$$\begin{aligned} Z_n^{(2)}(z_1,\bar{z}_1,z_2,\bar{z}_2) &\simeq \int_{\mathrm{Sp}(2n)} \mathrm{d}U\, \mathrm{e}^{-g^{-1}r_s^2 4n} \det{}^{N/2} \begin{pmatrix} \bar{Z} & r_s U \\ -r_s U^\dagger & Z \end{pmatrix} \\ &\simeq \int_{\mathrm{Sp}(2n)} \mathrm{d}U\, \exp\left[g^{-1}\mathrm{tr}\left(U^\dagger \bar{Z} U Z\right)\right]. \end{aligned} \tag{36}$$

When we introduce $z=(z_1+z_2)/2$, $\omega = z_1 - z_2$, and $s = \mathrm{diag}(1,-1)\otimes \mathbb{I}_{2n}$, we have $Z = z\mathbb{I}_{4n} + \frac{1}{2}\omega s$ and hence

$$Z_n^{(2)}(z_1,\bar{z}_1,z_2,\bar{z}_2) \simeq \mathrm{e}^{g^{-1}4n|z|^2} Y_{\mathrm{Sp}(n)}\left(|\omega|^2\right) \quad \text{where} \quad Y_{\mathrm{Sp}(n)}\left(|\omega|^2\right) = \int_{\mathrm{Sp}(2n)} \mathrm{d}U\, \exp\left[\frac{|\omega|^2}{4g}\mathrm{tr}\left(U^\dagger s U s\right)\right]. \tag{37}$$

Observe that for $U\in\mathrm{Sp}(2n)$, $U^\dagger s U$ lies on the symplectic Grassmannian $\mathrm{Sp}(2n)/[\mathrm{Sp}(n)\times \mathrm{Sp}(n)]$. Thus, the target space of this NLσM is the symplectic Grassmannian. In the following, we calculate this integral in the regime $|\omega|^2 \gg g$.

2.3.1. Cosine-sine decomposition. Analogous to the singular-value decomposition used in section 2.2, we find that a cosine-sine (CS) decomposition for the symplectic group is effective in calculating the second-order characteristic polynomial $Z_n^{(2)}$. The CS decomposition of a symplectic unitary matrix $U\in\mathrm{Sp}(2n)$ is described below [87]. We start with the following parametrization,

$$U = \begin{pmatrix} u_1 & 0 \\ 0 & u_2 \end{pmatrix} \begin{pmatrix} \cos\Theta & \sin\Theta \\ -\sin\Theta & \cos\Theta \end{pmatrix} \begin{pmatrix} v_1 & 0 \\ 0 & v_2 \end{pmatrix}, \tag{38}$$

with

$$\Theta = \mathrm{diag}(\theta_1,\theta_1,\ldots,\theta_n,\theta_n), \text{where } \theta_i\in[0,\pi),\ u_{1,2},v_{1,2}\in\mathrm{Sp}(n). \tag{39}$$

Notice that each angle is repeated twice. One can regard each θ_i as the commuting part of the 2×2 matrix representation of a quaternion. While $u_{1,2}$ and $v_{1,2}$ are generic matrices in $\mathrm{Sp}(n)$, they must be compensated by an $\mathrm{Sp}(1)^{\otimes n}$ phase factor inside the CS matrix. A parametrization for $\mathrm{Sp}(1)\cong S^3$ is $\mathrm{e}^{\mathrm{i}\phi(\mathbf{m}\cdot\Sigma)}$ with $\phi\in[0,\pi]$ and $\mathbf{m}\in\mathbb{R}^3$ satisfying $|\mathbf{m}|^2=1$ (i.e. $\mathbf{m}\in S^2$). We thus obtain a new CS decomposition without redundancy by

$$U = \begin{pmatrix} u_1 & 0 \\ 0 & u_2 \end{pmatrix} \begin{pmatrix} \cos\Theta\exp(\mathrm{i}\Phi\mathbf{M}\cdot\Sigma) & \sin\Theta \\ -\sin\Theta & \cos\Theta\exp(-\mathrm{i}\Phi\mathbf{M}\cdot\Sigma) \end{pmatrix} \begin{pmatrix} v_1 & 0 \\ 0 & v_2 \end{pmatrix}, \tag{40}$$

with

$$u_{1,2}\in \mathrm{Sp}(n)/\mathrm{Sp}(1)^{\otimes n}, \quad v_{1,2}\in\mathrm{Sp}(n); \tag{41}$$

$$\mathbf{M}\cdot\Sigma = \mathrm{diag}(\mathbf{m}_1\cdot\Sigma,\ldots,\mathbf{m}_n\cdot\Sigma), \quad \Phi = \mathrm{diag}(\phi_1,\phi_1,\ldots,\phi_n,\phi_n) \quad \left[\mathbf{m}_i\in S^2,\phi_i\in[0,\pi]\right]. \tag{42}$$

Now, we proceed to derive the Haar measure in terms of these new variables. Let Λ be the CS matrix. By using the invariance properties of the Haar measure, it is sufficient to consider a neighborhood of $u_{1,2} = v_{1,2} = \mathbb{I}_{2n}$, leading to

$$U^\dagger \mathrm{d}U = \begin{pmatrix} \mathrm{d}v_1 & 0 \\ 0 & \mathrm{d}v_2 \end{pmatrix} + \Lambda^\dagger \begin{pmatrix} \mathrm{d}u_1 & 0 \\ 0 & \mathrm{d}u_2 \end{pmatrix} \Lambda + \Lambda^\dagger \mathrm{d}\Lambda. \tag{43}$$

The calculations follow quite similarly to the unitary case from here on. The contribution from $\Lambda^\dagger \mathrm{d}\Lambda$ is simply an extension of the measure for Sp(2) matrices given in [88]. The second term is the non-trivial part, which by comparison to the unitary case contributes $\Delta(\cos^2\Theta)^4$. Finally, the Haar measure is obtained as

$$\mathrm{d}U^{\mathrm{Haar}} \propto \mathrm{d}u_1^{\mathrm{Haar}} \mathrm{d}u_2^{\mathrm{Haar}} \mathrm{d}v_1^{\mathrm{Haar}} \mathrm{d}v_2^{\mathrm{Haar}} |\Delta\left(\cos^2\Theta\right)|^4 \prod_{i=1}^{n} \sin^3(2\theta_i) \sin^2(\phi_i)\, \mathrm{d}\theta_i\, \mathrm{d}\phi_i\, \mathrm{d}^2\mathbf{m}_i. \tag{44}$$

Now, we recall the saddle-point integral in equation (37). The integrand in terms of the new variables is

$$\exp\left(\frac{|\omega|^2}{4g} \mathrm{tr}\left(UsU^\dagger s\right)\right) = \exp\left(\frac{|\omega|^2}{2g} \mathrm{tr}\left(\cos 2\Theta\right)\right). \tag{45}$$

Thus, ignoring irrelevant overall constants, we have

$$\begin{aligned} Y_{\mathrm{Sp}(n)}\left(|\omega|^2\right) &\simeq \int_0^\pi \prod_{i=1}^{n} \mathrm{d}\theta_i \sin^3(2\theta_i) \exp\left(\frac{|\omega|^2}{2g} \mathrm{tr}\cos 2\Theta\right) |\Delta\left(\cos^2\Theta\right)|^4 \\ &= \int_{-1}^{1} \prod_{i=1}^{n} \mathrm{d}\lambda_i \left(1-\lambda_i^2\right) \mathrm{e}^{|\omega|^2 \sum_i \lambda_i} |\Delta(\lambda)|^4, \end{aligned} \tag{46}$$

where we set $g = 1$ for simplicity and introduce $\lambda_i = \cos 2\theta_i$, satisfying $\mathrm{tr}\cos 2\Theta = 2\sum_i \lambda_i$. To make a comparison with Selberg integrals, we make the shift $\lambda \to 1-\lambda$ and then rescale $\lambda \to 2\lambda$, resulting in

$$Z_n^{(2)}(z_1, \bar{z}_1, z_2, \bar{z}_2) \simeq \mathrm{e}^{4n|z|^2} Y_{\mathrm{Sp}(n)}\left(|\omega|^2\right), \tag{47}$$

$$Y_{\mathrm{Sp}(n)}\left(|\omega|^2\right) \simeq \mathrm{e}^{n|\omega|^2} \int_0^1 \prod_{i=1}^{n} \mathrm{d}\lambda_i\, \lambda_i (1-\lambda_i)\, \mathrm{e}^{-2|\omega|^2 \sum_i \lambda_i} |\Delta(\lambda)|^4. \tag{48}$$

In figure 4, we plot the analytical expression in equation (47) of the second-order characteristic polynomial for various values of N and n as a function of $|z_2 - z_1|$. We also compare the analytical result in equation (47) with numerical results where we numerically generate non-Hermitian random matrices from the Gaussian ensemble in equation (2) and calculate the characteristic polynomial. Here, it should be noted that equation (47) is valid only for large N although it allows us to access the small $|\omega|$ regime, which is relevant for level repulsion. While the numerics for small N deviates from equation (47) for large z_2, it is consistent with equation (47) for large enough N and for small enough z_2.

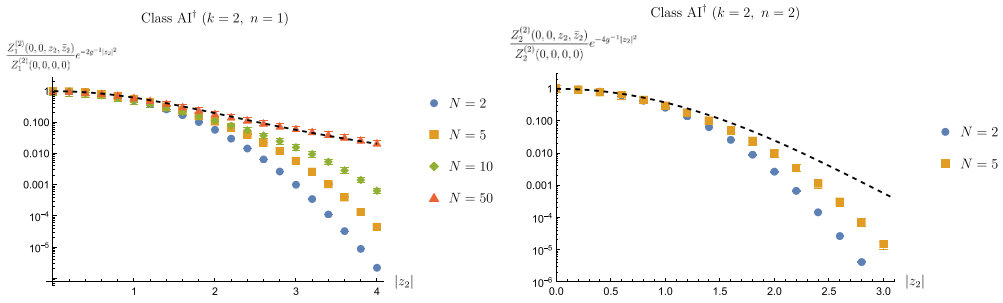

Figure 4. Logarithmic plot of the two-point characteristic polynomial in class AI†. We plot the expression $\frac{Z_n^{(2)}(0,0,z_2,\bar{z}_2)}{Z_n^{(2)}(0,0,0,0)}\mathrm{e}^{-2ng^{-1}|z_2|^2}$ instead of $Z_n^{(2)}(0,0,z_2,\bar{z}_2)$ for better visualization. For each value of $N=2$ and $N=5$, we collect 10^6 realizations of non-Hermitian random matrices, while for $N=10$ and $N=50$ we collect 5×10^6 realizations. In all cases, we use $g=2$. The solid markers show the numerically computed ensemble-averaged moments of characteristic polynomials. The black dashed curves show the same quantity calculated with the NLσM for large N in equation (47).

2.3.2. Two-point correlation function. We now discuss the two-point correlation function. The two-point correlation function is obtained from the second-order characteristic polynomial $Z_n^{(2)}$ by [71, 76]

$$\pi^2 R_2(z_1,\bar{z}_1,z_2,\bar{z}_2) = \lim_{n\to0}\frac{1}{n^2}\partial_{z_1}\partial_{\bar{z}_1}\partial_{z_2}\partial_{\bar{z}_2}Z_n^{(2)}(z_1,\bar{z}_1,z_2,\bar{z}_2), \tag{49}$$

where $Z_n^{(2)}$ is given by equation (18) with $k=2$. Using the fact that $Z_n^{(2)}$ factorizes into a z-dependent and ω-dependent part, we can simplify this as follows,

$$\begin{aligned}\pi^2 R_2(z_1,\bar{z}_1,z_2,\bar{z}_2) &= \lim_{n\to0}\frac{1}{n^2}\left(\partial_\omega^2-\partial_{2z}^2\right)\left(\partial_{\bar{\omega}}^2-\partial_{2\bar{z}}^2\right)\mathrm{e}^{4n|z|^2}Y_{\mathrm{Sp}(n)}\left(|\omega|^2\right)\\ &= 2+\lim_{n\to0}\frac{1}{n^2}\partial_\omega^2\partial_{\bar{\omega}}^2 Y_{\mathrm{Sp}(n)}\left(|\omega|^2\right).\end{aligned} \tag{50}$$

To evaluate R_2, we go back to equation (47) and analyze its behavior in the limit $n\to0$. It is difficult to evaluate this integral exactly on the domain $[0,1]^n$. However, we aim to evaluate it only up to order n^2. For this purpose, we can expand the domain to $[0,\infty]^n$ and then systematically add or subtract corrections at increasing orders in n. Only finitely many terms in this series survive at order n^2. To perform this procedure, we rewrite the contour of integration in equation (47) as a sum over two contours, $\int_0^1 \mathrm{d}\lambda \to \int_0^\infty \mathrm{d}\lambda - \int_1^\infty \mathrm{d}\lambda$. This gives

$$\begin{aligned}Y_{\mathrm{Sp}(n)}\left(|\omega|^2\right) &\simeq \mathrm{e}^{n\frac{t}{2}}\int_0^\infty\prod_{i=1}^n \mathrm{d}\lambda_i\,|\lambda_i(1-\lambda_i)|\,(1-\Theta(\lambda_i-1))\,\mathrm{e}^{-t\sum_i\lambda_i}|\Delta(\lambda)|^4\\ &\simeq \mathrm{e}^{4n|z|^2}\mathrm{e}^{n\frac{t}{2}}\sum_{p=0}^n\binom{n}{p}(-1)^p\int_1^\infty\prod_{i=1}^p\mathrm{d}x_i\,|x_i(1-x_i)|\,\mathrm{e}^{-t\sum_i x_i}\\ &\times\int_0^\infty\prod_{i=1}^{n-p}\mathrm{d}y_i\,|y_i(1-y_i)|\,\mathrm{e}^{-t\sum_i y_i}|\Delta(x,y)|^4\end{aligned} \tag{51}$$

with $t = 2|\omega|^2$. For large t, the x and y variables accumulate near the peak of the weight function $|\lambda(1-\lambda)|e^{-t\lambda}$ within their respective domain. To the leading order in $1/t$, these are simply located at $x = 1$ and $y = 0$, respectively, and hence we can make the approximation $\Delta(x,y) \simeq \Delta(x)\Delta(y)$. Let us focus on the y-integral. Since the y variables accumulate close to the origin, we can approximate $|y_i(1-y_i)| \simeq y_i$. Thus, we have

$$\int_0^\infty \prod_{i=1}^{n-p} \mathrm{d}y_i\, y_i\, \mathrm{e}^{-t\sum_i y_i} |\Delta(y)|^4 = \left(\frac{1}{t}\right)^{2(n-p)^2} \Gamma(3)^{p-n} \prod_{k=1}^{n-p} \Gamma(2k)\Gamma(1+2k)$$
$$\simeq \left(\frac{1}{t}\right)^{2(n-p)^2} \Gamma(3)^{p} \prod_{k=n-p+1}^{n} \left(\Gamma(2k)\Gamma(1+2k)\right)^{-1}. \tag{52}$$

After taking the $\binom{n}{p}$ factor into account, only $p = 0, 1$ terms survive at order n^2. On the other hand, the x-integral for $p = 0$ is trivially 1. For $p = 1$, it is

$$\int_1^\infty \mathrm{d}x_1\, x_1\,(x_1-1)\,\mathrm{e}^{-tx_1} = \frac{\mathrm{e}^{-t}(t+2)}{t^3}. \tag{53}$$

Thus, we have

$$Y_{\mathrm{Sp}(n)}\left(|\omega|^2\right) \simeq \mathrm{e}^{n\frac{t}{2}} \left(\frac{1}{t^{2n^2}} - \frac{4n^2\mathrm{e}^{-t}(t+2)}{t^5}\right)$$
$$\simeq \left(1 + \frac{nt}{2} + \frac{n^2t^2}{8} - 2n^2\ln t - \frac{4n^2\mathrm{e}^{-t}}{t^4}\right). \tag{54}$$

We rewrite equation (49) in terms of $\partial_\omega, \partial_z, \partial_{\bar\omega}$ and $\partial_{\bar z}$ to obtain

$$\pi^2 R_2(z_1,\bar z_1,z_2,\bar z_2) = \lim_{n\to 0}\frac{1}{n^2}\left(\partial_\omega^2 - \partial_{2z}^2\right)\left(\partial_{\bar\omega}^2 - \partial_{2\bar z}^2\right)\mathrm{e}^{4n|z|^2}\left(1 + \frac{nt}{2} + \frac{n^2t^2}{8} - 2n^2\ln t - \frac{4n^2\mathrm{e}^{-t}}{t^4}\right)$$
$$= 2 + \lim_{n\to 0}\frac{1}{n^2}\partial_\omega^2\partial_{\bar\omega}^2\left(1 + n|\omega|^2 + \frac{n^2|\omega|^4}{2} - 2n^2\ln\left(|\omega|^2\right) - \frac{n^2\mathrm{e}^{-2|\omega|^2}}{4|\omega|^8}\right). \tag{55}$$

Then, the two-point correlation function is obtained from equation (49), to leading order in $1/|\omega|$, as

$$\pi^2 R_2^{\mathrm{AI}^\dagger}(\omega) \simeq 4\left(1 - \frac{\mathrm{e}^{-2|\omega|^2}}{|\omega|^4}\right). \tag{56}$$

A similar saddle-point integral was also calculated in [74] (see appendix A for details). However, the relevant parameter μ is assumed to be real in [74], while it should be imaginary in our calculations. For comparison, we also analytically present the two-point correlation function $R_2(z_1,\bar z_1,z_2,\bar z_2)$ for 2×2 non-Hermitian random matrices in class $\mathrm{AI}^\dagger$ in appendix C.

In figure 5, we compare the result in equation (56) with numerical calculations. We recall that the regime of validity for this result is $\sqrt{g} \ll |z_1 - z_2|$ and $|z_1|, |z_2| \ll \sqrt{gN/2}$, although in this regime the effect of level repulsion is very small and difficult to detect numerically. A more interesting regime is $|z_1 - z_2| \simeq \sqrt{g}$. In this regime, our result for the two-point correlation function appears to deviate from the numerics substantially. In contrast, for the case of the one-point function and the density of states, in section 2.2.1, the analytical result in equation (33)

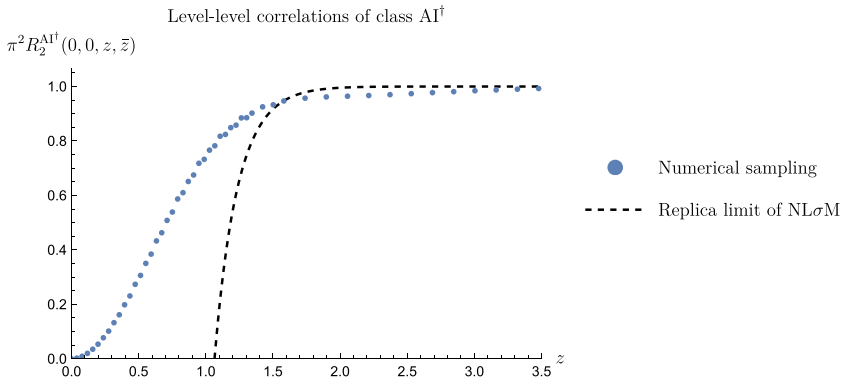

Figure 5. Comparison between the analytical result in equation (56) and the two-point correlation function obtained from numerical calculations. The numerical results are obtained by 2×10^4 realizations of $10^3 \times 10^3$ non-Hermitian random matrices in class AI† sampled according to equation (2) with $g = 2$.

appear to do a better job even outside of the regime of its validity. Taking equation (47) as a starting point, future work may investigate other contributions and provide important insights into the correlations of nearby eigenvalues in class AI†. Moreover, as we discussed previously at the end of section 2.2.1, we should explore more systematic approaches to taking the replica limit.

3. NLσM for class AII†

3.1. Replica space matrix integral for characteristic polynomials

Non-Hermitian matrices in class AII† respect TRS† with sign $\mathcal{T}^2 = -1$. We choose the symmetry operator to be $\mathcal{T} = \Sigma^y \mathcal{K}$, with complex conjugation $\mathcal{K}$ and $\Sigma^y = \sigma^y \otimes \mathbb{I}_N$. Thus, the symmetry condition reads

$$H^\dagger = \mathcal{T} H \mathcal{T}^{-1}, \quad \text{i.e.,} \quad \Sigma^y H^T \Sigma^y = H. \tag{57}$$

Here, H is a $2N \times 2N$ complex matrix. The symmetry condition may equivalently be expressed by representing H as follows,

$$H = \begin{pmatrix} a & b \\ c & a^T \end{pmatrix} \text{ where } a, b, c \in \mathbb{C}^{N\times N} \text{ and } b^T = -b,\ c^T = -c. \tag{58}$$

The Gaussian probability measure on H is given as follows,

$$\begin{aligned} P(H)\,\mathrm{d}H &= \mathrm{d}H \exp\left[-g^{-1} \mathrm{tr}\, H^\dagger H\right] \\ &= \mathcal{N}_{\mathrm{AII}^\dagger} \prod_{i,j=1}^{N} \mathrm{d}a_{ij} \mathrm{d}a_{ij}^* \prod_{1\leqslant i<j\leqslant N} \mathrm{d}b_{ij} \mathrm{d}b_{ij}^* \mathrm{d}c_{ij} \mathrm{d}c_{ij}^* \\ &\quad \times \exp\left[-2g^{-1}\left(\sum_{i,j=1}^{N} |a_{ij}|^2 + \sum_{1\leqslant i<j\leqslant N} \left(|b_{ij}|^2 + |c_{ij}|^2\right)\right)\right], \end{aligned} \tag{59}$$

where g parameterizes the width of the Gaussian and the normalization $\mathcal{N}_{\mathrm{AII}^\dagger}$ is defined by setting $\int dHP(H) = 1$. As before, the general characteristic polynomial for k-point functions is defined as in equation (3). We first focus on the $k = 1$ case and then generalize to $k > 1$. After rewriting the determinants in terms of Grassmann variables, the replica characteristic polynomial for the one-point function is given by

$$Z_n^{(1)}(z,\bar{z}) = \int \mathrm{d}HP(H) \int \mathrm{d}\psi\, \mathrm{d}\bar{\psi}\, \mathrm{d}\chi\, \mathrm{d}\bar{\chi} \times \exp\left[-\bar{\psi}_a^i \left(z\delta^{ij}\delta^{ab} - H^{ij}\delta^{ab}\right)\psi_a^j - \bar{\chi}_a^i \left(\bar{z}\delta^{ij}\delta^{ab} - \left(H^\dagger\right)^{ij}\delta^{ab}\right)\chi_a^j\right], \tag{60}$$

where the indices i, j now run from 1 to $2N$, and a, b run from 1 to n. Now, we account for the symmetry of H and distill the relevant fermionic degrees of freedom by noting

$$\bar{\psi}_a^i H^{ij}\psi_a^j = -\operatorname{tr}\left(H\psi_a\bar{\psi}_a^T\right) = +\operatorname{tr}\left(H\Sigma^y\bar{\psi}_a\psi_a^T\Sigma^y\right) = -\operatorname{tr}\left(H\lceil\psi_a\bar{\psi}_a^T\rceil\right), \tag{61}$$

where we define the modified symmetric part of the fermion bilinear as

$$\lceil\psi_a\bar{\psi}_a^T\rceil = \frac{1}{2}\left(\psi_a\bar{\psi}_a^T + \left(\Sigma^y\psi_a\bar{\psi}_a^T\Sigma^y\right)^T\right) = \frac{1}{2}\left(\psi_a\bar{\psi}_a^T - \Sigma^y\bar{\psi}_a\psi_a^T\Sigma^y\right). \tag{62}$$

Indeed, the modified symmetric part respects TRS† in class AII†: $\Sigma^y\lceil\psi_a\bar{\psi}_a^T\rceil^T\Sigma^y = \lceil\psi_a\bar{\psi}_a^T\rceil$. In perfect analogy to class AI† (see section 2.1), we integrate out the H variables and are left with the following integral,

$$Z_n^{(1)}(z,\bar{z}) = \int \mathrm{d}\psi\, \mathrm{d}\bar{\psi}\, \mathrm{d}\chi\, \mathrm{d}\bar{\chi}\, \exp\left[g\operatorname{tr}\left(\lceil\chi_a\bar{\chi}_a^T\rceil\lceil\psi_b\bar{\psi}_b^T\rceil\right) + \bar{z}\operatorname{tr}\left(\lceil\chi_a\bar{\chi}_a^T\rceil\right) + z\operatorname{tr}\left(\lceil\psi_a\bar{\psi}_a^T\rceil\right)\right]. \tag{63}$$

We expand the four-fermion term as

$$g\operatorname{tr}\left(\lceil\chi_a\bar{\chi}_a^T\rceil\lceil\psi_b\bar{\psi}_b^T\rceil\right) = \frac{1}{2}g\left[-\left(\bar{\psi}_b^T\chi_a\right)\left(\bar{\chi}_a^T\psi_b\right) + \left(\psi_b^T\Sigma^y\chi_a\right)\left(\bar{\chi}_a^T\Sigma^y\bar{\psi}_b\right)\right]. \tag{64}$$

We introduce flavor-space matrices Q and $R \in \mathbb{C}^{n\times n}$ to decouple, respectively, the first and second terms in equation (64),

$$\exp\left[-\frac{1}{2}g\operatorname{Tr}\left(\left(\bar{\psi}^T\chi\right)\left(\bar{\chi}^T\psi\right)\right)\right] \propto \int \mathrm{d}Q \exp\left[-\frac{1}{2}g^{-1}\operatorname{Tr}\left(QQ^\dagger\right) - \frac{1}{2}\operatorname{Tr}\left(\bar{\psi}^T\chi Q^\dagger\right) + \frac{1}{2}\operatorname{Tr}\left(Q\bar{\chi}^T\psi\right)\right]. \tag{65}$$

Similarly, we have

$$\exp\left[\frac{1}{2}g\operatorname{Tr}\left(\left(\psi^T\Sigma^y\chi\right)\left(\bar{\chi}^T\Sigma^y\bar{\psi}\right)\right)\right] \propto \int \mathrm{d}R \exp\left[-\frac{1}{2}g^{-1}\operatorname{Tr}\left(RR^\dagger\right) - \frac{1}{2}\operatorname{Tr}\left(R^\dagger\psi^T\Sigma^y\chi\right) - \frac{1}{2}\operatorname{Tr}\left(\bar{\chi}^T\Sigma^y\bar{\psi}R\right)\right]. \tag{66}$$

Following similar steps as before, we express the characteristic polynomial as

$$Z_n^{(1)}(z,\bar{z}) \simeq \int_{\mathbb{R}^{2n\times 2n}} \mathrm{d}\mathcal{Q}\, \mathrm{e}^{-g^{-1}\operatorname{tr}\mathcal{Q}^T\mathcal{Q}} \det{}^N \begin{pmatrix} -z & \mathcal{Q} \\ \mathcal{Q}^T & \bar{z} \end{pmatrix}. \tag{67}$$

Now, we generalize this expression to the k-point characteristic polynomial. The procedure is largely identical to the one above, resulting in

$$Z_n^{(k)}(z_1,\bar{z}_1,\ldots,z_k,\bar{z}_k) = \int_{\mathbb{R}^{2nk\times 2nk}} \mathrm{d}\mathcal{Q}\, \mathrm{e}^{-g^{-1}\mathrm{tr}\mathcal{Q}^T\mathcal{Q}}\, \det{}^N \begin{pmatrix} -Z & \mathcal{Q} \\ \mathcal{Q}^T & \bar{Z} \end{pmatrix}, \tag{68}$$

with

$$Z = \mathrm{diag}(z_1,\ldots,z_k)\otimes \mathbb{I}_{2n}. \tag{69}$$

In the subsequent sections, we will compute this integral for $k=1$ and $k=2$ under suitable limits.

3.2. One-point characteristic polynomial

We study the first-order characteristic polynomial $Z_n^{(1)}(z,\bar{z})$ in more detail and use it to derive the density of states for class AII†. First, we extract only the dominant contribution for large N. In this limit, the integral in equation (67) can be approximated by integrating over the saddle point. The saddle-point equation is

$$\mathcal{Q}^T\mathcal{Q} = \left(gN - |z|^2\right)\mathbb{I}_{2n}. \tag{70}$$

For $|z| < \sqrt{gN}$, it is solved by $\mathcal{Q} = \sqrt{gN-|z|^2}\,O$, with $O\in \mathrm{O}(2n)$. Dropping the overall factors irrelevant in the replica limit, we get $Z_n^{(1)}(z,\bar{z}) \simeq \mathrm{e}^{2ng^{-1}|z|^2}$, which gives $\pi R_1(z,\bar{z}) = 2g^{-1}$ from equation (26). This is consistent with numerical calculations and Girko's circular law [8].

Now, let us study the characteristic polynomial $Z_n^{(1)}(z,\bar{z})$ in more detail without any approximations. Below, we assume $g=1$ for simplicity. Notice that the integrand in equation (67) remains invariant if we multiply $\mathcal{Q}$ by an orthogonal matrix on the left or on the right. Thus, we can reduce the matrix integral to an integral over singular values of Q. Let the singular-value decomposition of $\mathcal{Q}\in\mathbb{R}^{2n\times 2n}$ be

$$\mathcal{Q} = U\Lambda V; \qquad U,V\in \mathrm{O}(2n), \qquad \Lambda = \mathrm{diag}\left(\lambda_1^{\frac{1}{2}},\ldots,\lambda_{2n}^{\frac{1}{2}}\right) \quad (\lambda_a\geqslant 0). \tag{71}$$

The integration measure on $\mathcal{Q}$ is transformed into the following measure on U, V, and Λ,

$$\mathrm{d}Q = \mathrm{d}U\mathrm{d}V|\Delta(\lambda)|\prod_{a=1}^{2n}\mathrm{d}\lambda_a\,\lambda_a^{-\frac{1}{2}}, \quad \Delta(\lambda) = \prod_{a>b}^{n}(\lambda_a-\lambda_b). \tag{72}$$

Since the integrand is independent of U and V, the integrals over U and V simply give the volume of $\mathrm{O}(2n)$. This is an irrelevant overall factor in the replica limit and hence ignored. The remaining integral is

$$Z_n^{(1)}(z,\bar{z}) \simeq \int_0^\infty \prod_{a=1}^{2n}\mathrm{d}\lambda_a I(\lambda_a)\,\lambda_a^{-\frac{1}{2}}|\Delta(\lambda)|, \qquad I(\lambda) = \mathrm{e}^{-\lambda}\left(\lambda+|z|^2\right)^N. \tag{73}$$

We refer the reader to [78, 79] for other results on this quantity.

In figure 6, we plot the analytical expression in equation (73) of the first-order characteristic polynomial for various values of N and n as a function of $|z|$. We also compare the analytical result in equation (73) with numerical results where we numerically generate non-Hermitian random matrices from the Gaussian ensemble in equation (59) and calculate the characteristic polynomial. For all values of N and n we studied, the analytical and numerical results are consistent.

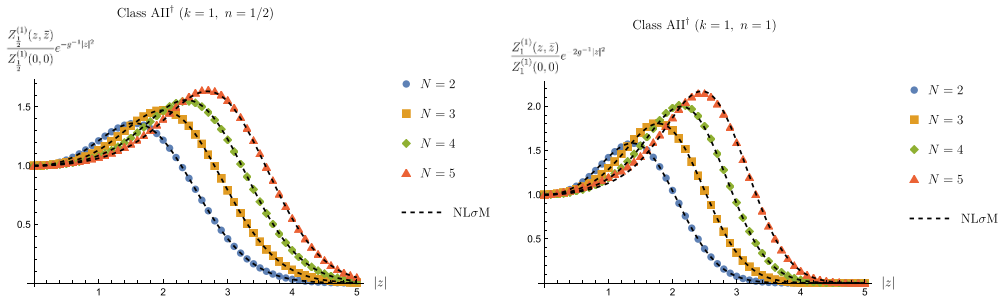

Figure 6. Plot of $\frac{Z_n^{(1)}(z,\bar{z})}{Z_n^{(1)}(0,0)}e^{-2ng^{-1}|z|^2}$ as a function of $|z|$ for class AII†. For each value of N, we sample 10^5 realizations of non-Hermitian random matrices according to equation (59) with $g=2$. The solid markers show the ensemble-averaged characteristic polynomials. The black dashed curves show the same quantity calculated by equation (73) obtained from the NLσM.

3.2.1. Density of states. As in the case of class AI†, we consider the large-N limit and approximate $I(\lambda)$ with an un-normalized Gaussian: $I(\lambda)\simeq N^N \mathrm{e}^{-\lambda_{\rm sp}}\exp(-\frac{(\lambda-\lambda_{\rm sp})^2}{2N})$. Here, $\lambda_{\rm sp}=N-|z|^2$ is the solution to the saddle-point equation $\partial_\lambda \ln I(\lambda)=0$. Rescaling $\lambda\to\lambda_{\rm sp}\lambda$, we obtain

$$Z_n^{(1)}(z,\bar{z})\simeq \mathrm{e}^{-2n\lambda_{\rm sp}}\lambda_{\rm sp}^{2n^2}\int_0^\infty\prod_{a=1}^{2n}\frac{\mathrm{d}\lambda_a}{\sqrt{|\lambda_a|}}\exp\left(-\frac{\lambda_{\rm sp}^2}{2N}(\lambda_a-1)^2\right)|\Delta(\lambda)|. \tag{74}$$

We rewrite the range of integration as $\int_0^\infty \mathrm{d}\lambda=\int_{-\infty}^\infty \mathrm{d}\lambda-\int_{-\infty}^0\mathrm{d}\lambda$. We consider the regime where $\frac{\lambda_{\rm sp}^2}{2N}$ is large enough so that x and y accumulate near the maxima of the weight function, i.e. 0 and 1, respectively. As such, we can approximate $\Delta(\lambda)\simeq\Delta(x)\Delta(y)$, and hence the x and y variables become decoupled, as follows:

$$\begin{aligned}Z_n^{(1)}(z,\bar{z})\simeq \mathrm{e}^{-2n\lambda_{\rm sp}}\lambda_{\rm sp}^{2n^2}\sum_p(-1)^p\binom{2n}{p}\int_{-\infty}^0\prod_{a=1}^{p}\frac{\mathrm{d}x_a}{\sqrt{|x_a|}}\exp\left(-\frac{\lambda_{\rm sp}^2}{2N}(x_a-1)^2\right)|\Delta(x)|\\ \times\int_{-\infty}^\infty\prod_{a=1}^{2n-p}\frac{\mathrm{d}y_a}{\sqrt{|y_a|}}\exp\left(-\frac{\lambda_{\rm sp}^2}{2N}(y_a-1)^2\right)|\Delta(y)|.\end{aligned} \tag{75}$$

Furthermore, in the y-integral, since the Gaussian is narrowly peaked at 1, we replace the factor of $|y_a|^{-\frac{1}{2}}$ in the integrand with 1. The remaining integral is a Selberg integral, evaluated exactly as

$$\int_{-\infty}^\infty\prod_{a=1}^{2n-p}\mathrm{d}y_a\exp\left(-\frac{\lambda_{\rm sp}^2}{2N}(y_a-1)^2\right)|\Delta(y)|\simeq\left(\frac{\lambda_{\rm sp}}{\sqrt{N}}\right)^{-\frac{(2n-p+1)(2n-p)}{2}}2^{\frac{3}{2}(2n-p)}\prod_{a=1}^{2n-p}\Gamma\left(1+\frac{1}{2}a\right). \tag{76}$$

We should check the coefficient of the pth term in this expansion and identify which terms survive in the limit $n\to 0$. The coefficient is $\binom{2n}{p}\prod_{a=1}^{2n-p}\Gamma\left(1+\frac{1}{2}a\right)$. At order n, the coefficients are 1, $2n$, and $-n/\sqrt{\pi}$ for $p=0$, 1, and 2, respectively, and zero for all $p\geqslant 3$. On the other hand, there is no x-integral for $p=0$. For $p=1$, it is

$$\int_{-\infty}^0\frac{\mathrm{d}x_1}{\sqrt{|x_1|}}\exp\left(-\frac{\lambda_{\rm sp}^2}{2N}(x_1-1)^2\right)\simeq\frac{\sqrt{\pi N}}{\lambda_{\rm sp}}\exp\left(-\frac{\lambda_{\rm sp}^2}{2N}\right)\quad\text{for}\quad\frac{\lambda_{\rm sp}^2}{2N}\gg 1. \tag{77}$$

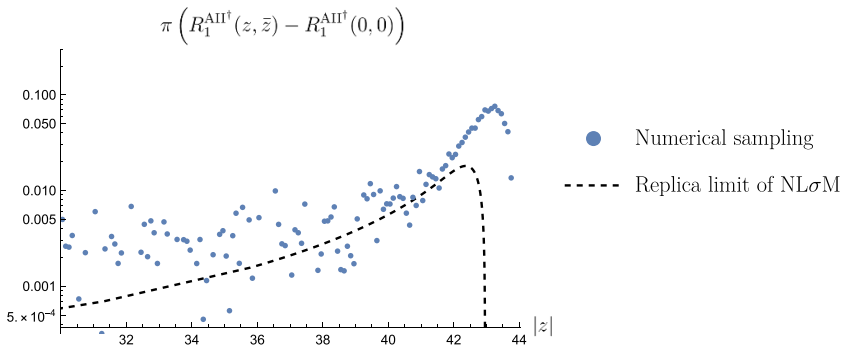

Figure 7. Comparison between the analytical result in equation (80) and the density of states obtained from numerical calculations. The numerical results are obtained by 10^4 realizations of $\left(2\times10^3\right)\times\left(2\times10^3\right)$ non-Hermitian random matrices in class AII† sampled according to equation (59) with $g=2$. Note that this is a logarithmic plot. This might cause the spread of the numerics in the plot.

For $p=2$, it is

$$\int_{-\infty}^{0}\frac{\mathrm{d}x_1}{\sqrt{|x_1|}}\int_{-\infty}^{0}\frac{\mathrm{d}x_2}{\sqrt{|x_2|}}\exp\left(-\frac{\lambda_{\mathrm{sp}}^2}{2N}\left[(x_1-1)^2+(x_2-1)^2\right]\right)|x_1-x_2|\simeq\frac{2N^2}{\lambda_{\mathrm{sp}}^4}\exp\left(-\frac{\lambda_{\mathrm{sp}}^2}{N}\right)\quad\text{for}\quad\frac{\lambda_{\mathrm{sp}}^2}{2N}\gg1. \tag{78}$$

Putting it all together, we have

$$Z_n^{(1)}(z,\bar{z})\simeq1-2n\lambda_{\mathrm{sp}}-n\ln\lambda_{\mathrm{sp}}-\frac{n}{\lambda_{\mathrm{sp}}}\sqrt{\frac{\pi N}{2}}\exp\left(-\frac{\lambda_{\mathrm{sp}}^2}{2N}\right)-\frac{n}{4\lambda_{\mathrm{sp}}^5}\sqrt{\frac{N^5}{\pi}}\exp\left(-\frac{\lambda_{\mathrm{sp}}^2}{N}\right)+\mathcal{O}\left(n^2\right). \tag{79}$$

Plugging this into equation (26) and keeping the leading-order terms, we obtain

$$\pi R_1(z,\bar{z})=2+\frac{1}{4u^2}-\sqrt{2\pi}\mathrm{e}^{-2u^2}\left(u+\frac{1}{4u}+\frac{1}{8u^3}\right)-\frac{\mathrm{e}^{-4u^2}}{8\sqrt{\pi}u^3}+\mathcal{O}\left(\frac{1}{u^5}\right), \tag{80}$$

where we introduce $u=\sqrt{N}-|z|$ as the distance of z from the edge of the spectrum and use $\lambda_{\mathrm{sp}}\simeq2u\sqrt{N}$. Similar to equation (33), we expect that the fermionic replica method can only reproduce the tail of the density of states for $|z|<\sqrt{gN}$ [71].

In figure 7, we compare the analytical result from equation (80), with the density of states obtained from numerical calculations. Notably, the positive term $+1/4u^2$ in equation (80) is unique to class AII† and does not appear in class A or AI†. As seen in figure 7, this term may explain the observed trend in the numerical data-specifically, the increase in the density of states near the edge of the spectrum. Similar to the discussion in Section 2.2.1, two caveats should be noted: (i) the validity of equation (80), which holds only for $|z|\ll\sqrt{gN}\approx44.72$, and (ii) the spread of numerical data due to the logarithmic scale of the plot. A more precise comparison with large-scale numerics, including corrections beyond the saddle-point approximation, as well as a more systematic approach to taking the replica limit, are left for future study.

3.3. Two-point characteristic polynomial

We recall the replica space matrix integral for the second-order characteristic polynomial in equation (68). For large N, we can approximate the $\mathcal{Q}$-integral by an integral over the saddle-point manifold of $\mathcal{Q}$. Unlike our discussion in section 3.2 for the density of states, Z and $\mathcal{Q}$ do not commute, which makes the saddle-point equation more involved. However, in the regime $z_{1,2} \ll \sqrt{gN}$, it is simplified to

$$\mathcal{Q}^T\mathcal{Q} = gN\mathbb{I}_{4n}, \tag{81}$$

which is solved as $\mathcal{Q} = \sqrt{gN}O$ with an orthogonal matrix $O \in \mathrm{O}(4n)$. The integral over the saddle-point manifold is

$$\begin{aligned} Z_n^{(2)}(z_1,\bar{z}_1,z_2,\bar{z}_2) &= \int_{\mathrm{O}(4n)} \mathrm{d}O\, \mathrm{e}^{-4nN} \det{}^N \begin{pmatrix} -Z & \sqrt{gN}O \\ \sqrt{gN}O^T & \bar{Z} \end{pmatrix} \\ &\simeq \int_{\mathrm{O}(4n)} \mathrm{d}O \exp\left[g^{-1}\mathrm{tr}\left(O^T Z O \bar{Z}\right)\right]. \end{aligned} \tag{82}$$

Here, we introduce $z = (z_1+z_2)/2$, $\omega = (z_1 - z_2)$, and $s = \mathrm{diag}(1,-1)\otimes\mathbb{I}_{2n}$, and then have $Z = z\mathbb{I}_{4n} + \frac{1}{2}\omega s$, leading to

$$Z_n^{(2)}(z_1,\bar{z}_1,z_2,\bar{z}_2) \simeq \mathrm{e}^{g^{-1}4n|z|^2} \int_{\mathrm{O}(4n)} \mathrm{d}O \exp\left[g^{-1}\mathrm{tr}\left(\frac{|\omega|^2}{4} O^T s O s\right)\right]. \tag{83}$$

When we define $W = O^T s O$, this change of variables maps the integration manifold to the orthogonal Grassmannian,

$$Z_n^{(2)}(z_1,\bar{z}_1,z_2,\bar{z}_2) \simeq \mathrm{e}^{g^{-1}4n|z|^2} \int_{\mathrm{O}(4n)/[\mathrm{O}(2n)\times\mathrm{O}(2n)]} \mathrm{d}W \exp\left[g^{-1}\mathrm{tr}\left(\frac{|\omega|^2}{4} W s\right)\right]. \tag{84}$$

3.3.1. Cosine-sine decomposition. We further simplify the above integrals by using the CS decomposition of the orthogonal group $\mathrm{O}(4n)$,

$$O = \begin{pmatrix} u_1 & 0 \\ 0 & u_2 \end{pmatrix} \begin{pmatrix} \cos\Theta & \sin\Theta \\ -\sin\Theta & \cos\Theta \end{pmatrix} \begin{pmatrix} v_1 & 0 \\ 0 & v_2 \end{pmatrix}, \tag{85}$$

with

$$\Theta = \mathrm{diag}(\theta_1,\ldots,\theta_{2n}), \qquad \theta_i \in [0,\pi), \qquad u_{1,2}, v_{1,2} \in \mathrm{O}(2n). \tag{86}$$

The integrand is only a function of Θ, not dependent on u and v,

$$\exp\left(\frac{|\omega|^2}{4}\mathrm{tr}\left(OsO^T s\right)\right) = \exp\left(\frac{|\omega|^2}{2}\cos 2\Theta\right), \tag{87}$$

where we have set $g = 1$ to lighten the notation. Now, we express the Haar measure on $\mathrm{O}(4n)$ in terms of u, v, and Θ. Due to the invariance properties of the Haar measure, we can assume that $u_{1,2}$ and $v_{1,2}$ are in the neighborhood of identity. Thus, the Haar measure in terms of u, v, and Θ is given as

$$\bigwedge_{4n\geqslant i>j\geqslant 1} \left(O^T \mathrm{d}O\right)_{ij} = \bigwedge_{k>l} (\mathrm{d}v_1)_{kl} (\mathrm{d}v_2)_{kl} \bigwedge_m \mathrm{d}\theta_m \bigwedge_{i>j} (\mathrm{d}u_1)_{ij} \wedge (\mathrm{d}u_2)_{ij}\, \Delta(\cos 2\Theta). \tag{88}$$

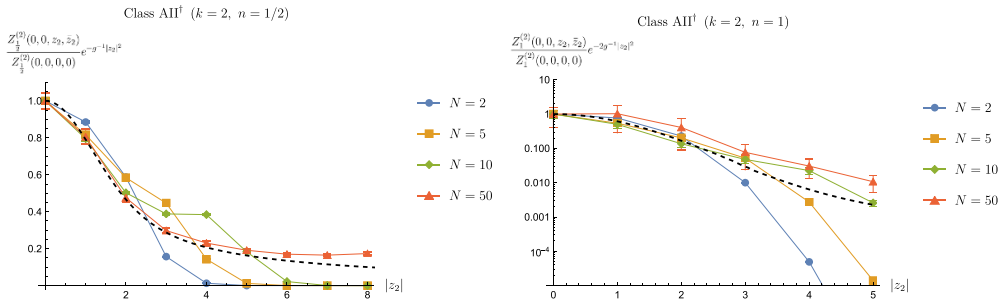

Figure 8. Plots of the two-point characteristic polynomial in class AII†. We plot the expression $\frac{Z_n^{(2)}(0,0,z_2,\bar{z}_2)}{Z_n^{(2)}(0,0,0,0)}\mathrm{e}^{-2ng^{-1}|z_2|^2}$ instead of $Z_n^{(2)}(0,0,z_2,\bar{z}_2)$ for better visualization. For each value of N, we sample 2×10^6 realizations of non-Hermitian random matrices in class AII†. In all cases, we use $g=2$. The solid markers show the ensemble-averaged characteristic polynomials. The black dashed curves show the same quantity calculated by the NLσM for large N in equation (90).

For u and v, the measure is just the Haar measure on O$(2n)$, which only contributes an irrelevant overall factor. The relevant part is the measure on Θ. Thus, we finally have

$$Z_n^{(2)}(z_1,\bar{z}_1,z_2\bar{z}_2)\simeq \mathrm{e}^{4n|z|^2}\int_0^\pi \mathrm{d}\Theta\,|\Delta(\cos 2\Theta)|\exp\left(\frac{|\omega|^2}{2}\sum_i\cos 2\theta_i\right). \tag{89}$$

Introducing $\lambda_i=\sin(\theta_i)^2$ and $t=|\omega|^2$, we further have

$$Z_n^{(2)}(z_1,\bar{z}_1,z_2,\bar{z}_2)\simeq \mathrm{e}^{4n|z|^2}Y_{\mathrm{O}(2n)}\left(|\omega|^2\right), \tag{90}$$

$$Y_{\mathrm{O}(m)}(t)=\mathrm{e}^{mt/2}\int_0^1\prod_{i=1}^m\mathrm{d}\lambda_i\;\left(\lambda_i(1-\lambda_i)\right)^{-\frac{1}{2}}\mathrm{e}^{-t\sum_i\lambda_i}|\Delta(\lambda)|. \tag{91}$$

In figure 8, we plot the analytical result in equation (90) for the second-order characteristic polynomial as a function of $|z_2-z_1|, N$, and n and compare this with numerically generated data. For the numerics, we sample non-Hermitian random matrices in class AII† from the Gaussian ensemble in equation (59) and calculate the characteristic polynomial by exact diagonalization. Note that while equation (90) is valid only for large N, it allows us to access the small $|z_1-z_2|$ regime, which is relevant for level repulsion. Indeed, in figure 8 we see that while the numerics deviates from equation (90) for small N and large z_2, it is consistent with equation (90) for large enough N and for small enough z_2.

3.3.2. Two-point correlation function. As before, we extend the range of integration from $[0,1]$ to $[0,\infty)$ and deform the integration contour for each λ_i as $\int_0^1\mathrm{d}\lambda\to\int_0^\infty\mathrm{d}\lambda-\int_1^\infty\mathrm{d}\lambda$. Now, we make several approximations. We observe that in each branch of the contour, the dominant contribution comes from the endpoints 0 and 1. At these endpoints, $(\lambda_i(1-\lambda_i))^{-\frac{1}{2}}$ can be approximated as $\lambda^{-\frac{1}{2}}$ and $(1-\lambda)^{-\frac{1}{2}}$. We can also factorize the Vandermonde determinant such that variables on different contours are decoupled. Introducing $t=|\omega|^2$, we thus have

$$\begin{aligned}Y_{\mathrm{O}(m)}(t)=\mathrm{e}^{mt/2}\sum_{p=0}^m\binom{m}{p}(-1)^p\int_0^\infty\prod_{i=1}^{m-p}\mathrm{d}y_i\;|y_i|^{-\frac{1}{2}}\mathrm{e}^{-t\sum_i y_i}|\Delta(y)|\\ \times\mathrm{e}^{-pt}\int_0^\infty\prod_{i=1}^p\mathrm{d}x_i\;|x_i|^{-\frac{1}{2}}\mathrm{e}^{-t\sum_i x_i}|\Delta(x)|.\end{aligned} \tag{92}$$

The y-integral is a Selberg integral evaluated as

$$\int_0^\infty \prod_{i=1}^{m-p} \mathrm{d}y_i \ |y_i|^{-\frac{1}{2}} \mathrm{e}^{-t\sum_i y_i} |\Delta(y)| = t^{-(m-p)^2/2} \frac{1}{\Gamma\left(\frac{3}{2}\right)^{m-p}} \prod_{k=1}^{m-p} \Gamma\left(\frac{k}{2}\right) \Gamma\left(1+\frac{k}{2}\right). \tag{93}$$

The combinatorial factor to be expanded in small n is then

$$F^p{}_n = \frac{\Gamma(m+1)}{\Gamma(p+1)\Gamma(m-p+1)} \prod_{k=m-p+1}^{m} \Gamma\left(\frac{k}{2}\right)^{-1} \Gamma\left(1+\frac{k}{2}\right)^{-1}. \tag{94}$$

At order n^2, the non-zero terms are $p = 0, 1, 2$. The relevant x-integrals for $p = 1$ and 2 are respectively

$$\int_0^\infty \mathrm{d}x_1 \ x_1^{-\frac{1}{2}} \mathrm{e}^{-tx_1} = \sqrt{\frac{\pi}{t}}, \tag{95}$$

$$\int_0^\infty \mathrm{d}x_1 \mathrm{d}x_2 \ (x_1 x_2)^{-\frac{1}{2}} \mathrm{e}^{-t(x_1+x_2)} |x_1 - x_2| = \frac{2}{t^2}. \tag{96}$$

Thus, to leading order in t, we have

$$Y_{\mathrm{O}(m)}(t) \simeq 1 + \frac{mt}{2} + \frac{m^2 t^2}{4} - \frac{m^2}{2} \ln t - \frac{m^2 \pi}{4} \frac{\mathrm{e}^{-t}}{t} + \frac{m^2}{16} \frac{\mathrm{e}^{-2t}}{t^4} + \mathcal{O}\left(m^3\right). \tag{97}$$

Now we use equation (49) to calculate the two-point function. Notice once again that the factorization of $Z_n^{(2)}$ into separate z-dependent and ω-dependent parts yields

$$\begin{aligned} \pi^2 R_2(z_1, \bar{z}_1, z_2, \bar{z}_2) &= \lim_{n\to 0} \frac{1}{n^2} \left(\partial_\omega^2 - \partial_{z_z}^2\right) \left(\partial_{\bar{\omega}}^2 - \partial_{z_{\bar{z}}}^2\right) e^{4n|z|^2} Y_{\mathrm{O}(2n)}\left(|\omega|^2\right) \\ &= 2 + \lim_{n\to 0} \frac{1}{n^2} \partial_\omega^2 \partial_{\bar{\omega}}^2 Y_{\mathrm{O}(2n)}\left(|\omega|^2\right). \end{aligned} \tag{98}$$

Combining this with the approximation for $Y_{\mathrm{O}(2n)}$ we obtain the following expression for the two-point function of class AII†

$$\pi^2 R_2(\omega) \simeq 4 - \pi |\omega|^2 \mathrm{e}^{-|\omega|^2}. \tag{99}$$

This is compatible with the saddle-point integral in [74] (see appendix A for details). For comparison, we also analytically present the two-point correlation function $R_2(z_1, \bar{z}_1, z_2, \bar{z}_2)$ for 4×4 non-Hermitian random matrices in class AII† in appendix C. In figure 9, we compare the analytical result in equation (99) and the numerically generated two-point correlation function.

Similar remarks that we made for figure 5 apply here. Namely, the analytical result in equation (99) deviates substantially from the numerics in the regime $|z_1 - z_2| \lesssim \sqrt{g}$. However, in future works, equation (90) can be used as a starting point to study this regime. Finally, as we discussed in section 2.2.1, 2.3.2, and 3.2.1, we should keep in mind that there may be more systematic ways of taking the replica limit.

4. Conclusion

In this work, we investigated the spectral properties of Gaussian non-Hermitian random matrices in symmetry classes AI† and AII†. Using the fermionic replica NLσMs, we computed the one-point and two-point characteristic polynomials. We compared our results with finite-N numerical calculations and found good agreements. The method developed in this work can be applied to other symmetry classes of non-Hermitian RMT [76]. Taking the replica limit, we also calculated the density of states and the two-point

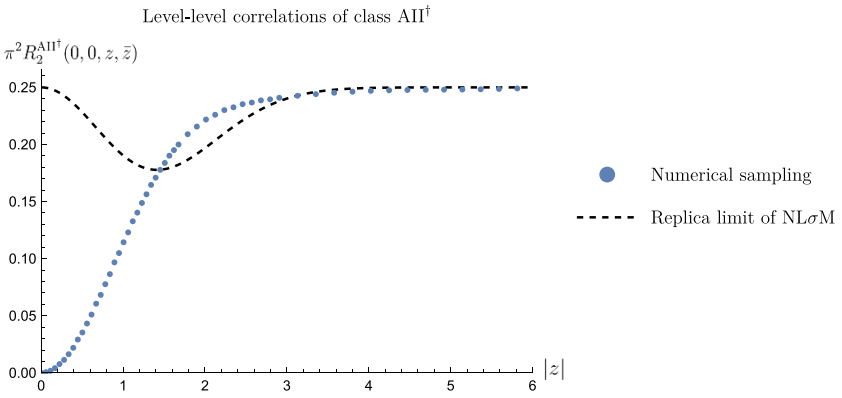

Figure 9. Comparison between the analytical result in equation (99) and the two-point correlation function obtained from numerical calculations. The numerical results are obtained by 10^4 realizations of $\left(2\times 10^3\right)\times\left(2\times 10^3\right)$ non-Hermitian random matrices in class AII† sampled according to equation (59) with $g=2$.

correlation functions. As discussed in section 2.2.1, there remains room for improvement on these calculations. Another important challenge is to establish the universality of level statistics. Our derivation of the NLσMs yields different target spaces for different symmetry classes which provides support to the universality conjecture. However, our treatment is currently limited to Gaussian ensembles. Extending our treatment to non-Gaussian ensembles will be necessary to rigorously establish universality. Further studies will be required to address this limitation. Lastly, it is interesting to explore applications of our results to physical systems, such as Lindblad superoperators.

Note added.—A part of this work was presented in [89]. When we were finalizing the draft, we learned about a related work [78]. After the initial submission of this work, we also learned about another related work [79].

Data availability statement

All data that support the findings of this study are included within the article (and any supplementary files).

Acknowledgments

We thank Ze Chen, Giorgio Cipolloni, and Jacobus Verbaarschot for helpful discussion. K K is supported by MEXT KAKENHI Grant-in-Aid for Transformative Research Areas A 'Extreme Universe' No. 24H00945. S R is supported by Simons Investigator Grant from the Simons Foundation (Grant No. 566116). We gratefully acknowledge support from the Simons Center for Geometry and Physics, Stony Brook University at which some of the research for this work was performed.

Appendix A. Saddle-point integral

A.1. Class AI†

We calculate the saddle-point integral using the results from [74], which computed the following sigma model matrix integral:

$$Y_{\mathrm{S}(n)}(-\mathrm{i}\mu) = \int_{\mathrm{S}(2n)/[\mathrm{S}(n)\times\mathrm{S}(n)]} \mathcal{D}W \exp\left[-\frac{\mathrm{i}\mu\alpha}{4}\mathrm{Tr}\,(sW)\right]. \tag{A1}$$

The group S(n) can be O(n), U(n), or Sp(n), corresponding to $\alpha = 2$, $\alpha = 2$, or $\alpha = 1$, respectively. When we define $W = U^\dagger sU$ and substitute $\mu = 2\mathrm{i}g^{-1}|\omega|^2$, this becomes almost the same matrix integral in equation (37). We note, however, that μ is assumed to be real in [74], while it should be imaginary in our calculations. Assuming that the measure is identical, we have the following expression for $Z_n^{(2)}$ up to z-independent factors that reduce to 1 in the replica limit,

$$Z_n^{(2)}(z_1,\bar{z}_1,z_2,\bar{z}_2) = \mathrm{e}^{4g^{-1}n|z|^2} Y_n\left(g^{-1}|\omega|^2\right). \tag{A2}$$

We rewrite R_2 in terms of Y_n and $\partial_\omega, \partial_z$, and so on, and assume $g = 1$ for simplicity, leading to

$$\begin{aligned}\pi^2 R_2(z_1,\bar{z}_1,z_2,\bar{z}_2) &= \lim_{n\to 0}\frac{1}{n^2}\left(\partial_\omega^2 - \partial_{2z}^2\right)\left(\partial_{\bar{\omega}}^2 - \partial_{2\bar{z}}^2\right)\mathrm{e}^{4n|z|^2} Y_n\left(|\omega|^2\right)\\ &= 2 + \lim_{n\to 0}\frac{1}{n^2}\partial_\omega^2\partial_{\bar{\omega}}^2 Y_n\left(|\omega|^2\right).\end{aligned} \tag{A3}$$

Hence, we only need to keep terms of order n^2 in Y_n. For the symplectic case, at large μ, we use the $\beta = 1$ result from [74]:

$$Y_{n\to 0}(-\mathrm{i}\mu) = 1 - \mathrm{i}\mu n + n^2\left(-\frac{\mu^2}{2} - 2\ln\mu + \frac{\mathrm{e}^{2\mathrm{i}\mu}}{4\mu^4}\right). \tag{A4}$$

In our calculations, we instead need $\mu = i\nu$, $\nu \in \mathbb{R}_{>0}$. The sign of the $\mathrm{e}^{2\mathrm{i}\mu}/\mu^4$ term is ambiguous for $\mu = i\nu$. We here choose the sign based on a physical expectation and replace $\ln\mu \to \ln|\mu|$. Then, we have

$$Y_{n\to 0}(\nu) = 1 + \nu n + n^2\left(\frac{\nu^2}{2} - 2\ln\nu - \frac{\mathrm{e}^{-2\nu}}{4\nu^4}\right) \tag{A5}$$

for $\nu \in \mathbb{R}_{>0}$. By using the above expression for Y_n, the term $z^2\partial_\omega^2 + \bar{z}^2\partial_{\bar{\omega}}^2$ should vanish in the $n \to 0$ limit. We are thus left with

$$\begin{aligned}\pi^2 R_2(z_1,\bar{z}_1,z_2,\bar{z}_2) &= 2 + \partial_\omega^2\partial_{\bar{\omega}}^2\left(\frac{\nu^2}{2} - 2\ln\nu - \frac{\mathrm{e}^{-2\nu}}{4\nu^4}\right)\\ &= 4 - \frac{4\mathrm{e}^{-2|\omega|^2}}{|\omega|^4} + \mathcal{O}\left(\frac{\mathrm{e}^{-|\omega|^2}}{|\omega|^2}\right) + \mathcal{O}\left(\frac{\mathrm{e}^{-2|\omega|^2}}{|\omega|^4}\right),\end{aligned} \tag{A6}$$

where we introduce $\omega = z_1 - z_2$ and $\nu = g^{-1}\omega\bar{\omega}$. While we here assume $g = 1$ for simplicity, the g dependence is recovered as

$$\pi^2 R_2(z_1,\bar{z}_1,z_2,\bar{z}_2) = 4g^{-2}\left(1 - \frac{\mathrm{e}^{-2g^{-1}|\omega|^2}}{g^{-2}|\omega|^4} + \mathcal{O}\left(\frac{\mathrm{e}^{-g^{-1}|\omega|^2}}{g^{-1}|\omega|^2}\right) + \mathcal{O}\left(\frac{\mathrm{e}^{-2g^{-1}|\omega|^2}}{g^{-2}|\omega|^4}\right)\right). \tag{A7}$$

A.2. Class AII†

For the orthogonal case, at large μ, we use the $\beta = 4$ result from [74]:

$$Y_{\mathrm{O}(2n)}(-\mathrm{i}\mu) = 1 - 2\mathrm{i}\mu n + 4n^2\left(-\frac{\mu^2}{2} - \frac{1}{2}\ln\mu + \Gamma^2(3/2)\frac{\mathrm{e}^{2\mathrm{i}\mu}}{2\mu} + \frac{\mathrm{e}^{4\mathrm{i}\mu}}{2^8\mu^4}\right) + \mathcal{O}\left(n^2\right) \tag{A8}$$

for $\mu \in \mathbb{R}$. As equation (A3), we rewrite the two-point correlation function in terms of z and ω derivatives and assume $g = 1$ for simplicity, leading to

$$\pi^2 R_2(z_1, \bar{z}_1, z_2, \bar{z}_2) = 2 + \lim_{n\to 0}\frac{1}{n^2}\partial_\omega^2\partial_{\bar{\omega}}^2 Y_{\mathrm{O}(2n)}\left(|\omega|^2/2\right). \tag{A9}$$

Thus, we have

$$\begin{aligned}\pi^2 R_2(z_1, \bar{z}_1, z_2, \bar{z}_2) =& \ 2 + 4\partial_\omega^2\partial_{\bar{\omega}}^2\left(\frac{|\omega|^4}{8} - \frac{1}{2}\ln\left(\frac{i|\omega|^2}{2}\right) - \frac{\pi}{}4\frac{\mathrm{e}^{-|\omega|^2}}{|\omega|^2} + \frac{\mathrm{e}^{-2|\omega|^2}}{2^4|\omega|^8}\right)\\ =& \ 4 - \pi|\omega|^2\mathrm{e}^{-|\omega|^2} + \mathrm{e}^{-2|\omega|^2}\mathcal{O}\left(\frac{1}{|\omega|^6}\right).\end{aligned} \tag{A10}$$

Putting the g dependence back by dimensional analysis, we have

$$\pi^2 R_2(z_1, \bar{z}_1, z_2, \bar{z}_2) = \ g^{-2}\left(4 - \pi g^{-1}|\omega|^2\mathrm{e}^{-g^{-1}|\omega|^2} + \mathrm{e}^{-2g^{-1}|\omega|^2}\mathcal{O}\left(\frac{1}{g^{-3}|\omega|^6}\right)\right). \tag{A11}$$

Appendix B. Jacobian of quaternion SVD

In this appendix, we derive the Jacobian of the singular value decomposition (SVD) of a quaternion matrix. Let Q be an $n \times n$ quaternion matrix. The SVD is given by

$$Q = U\Lambda V, \quad \Lambda = \mathrm{diag}\left(\sqrt{\lambda}_1, \ldots, \sqrt{\lambda}_n\right), \ \lambda_i \in \mathbb{R}_{\geqslant 0}, \ V \in \mathrm{Sp}(n), \ U \in \mathrm{Sp}(n)/\mathrm{Sp}(1)^{\oplus n}. \tag{B1}$$

The Euclidean measure on Q written as a differential form is $\bigwedge_c \bigwedge_{i,j} \mathrm{d}Q_{i,j}^{(c)}$ where the index $c = 0, \ldots, 3$ represents the various components of the quaternion numbers. This measure is invariant under multiplying Q on the left or right with a quaternion unitary matrix. We use this freedom to choose U, V in the neighborhood of identity. We then have

$$\mathrm{d}Q = \mathrm{d}U\Lambda + \Lambda\mathrm{d}V + \mathrm{d}\Lambda. \tag{B2}$$

Due to unitarity, we also have $\mathrm{d}U = -\mathrm{d}U^\dagger$ and $\mathrm{d}V = -\mathrm{d}V^\dagger$. In particular, this means that the diagonal of $\mathrm{d}U$ is zero and the real part of the diagonal of $\mathrm{d}V$ is zero. The Euclidean measure (up to an overall sign) is therefore given as

$$\begin{aligned}\bigwedge_{c=0}^{3}\bigwedge_{i,j}\mathrm{d}Q_{i,j}^{(c)} =& \left(\bigwedge_i \mathrm{d}\sqrt{\lambda}_i\right)\left(\bigwedge_{c=1}^{3}\bigwedge_i \mathrm{d}V_{ii}^{(c)}\sqrt{\lambda}_i\right)\left(\bigwedge_{c=0}^{3}\bigwedge_{i<j}\left(\mathrm{d}U_{ij}^{(c)}\sqrt{\lambda}_j + \sqrt{\lambda}_i\mathrm{d}V_{ij}^{(c)}\right) \wedge \left(\mathrm{d}U_{ij}^{(c)}\sqrt{\lambda}_i + \sqrt{\lambda}_j\mathrm{d}V_{ij}^{(c)}\right)\right)\\ =& \left(\bigwedge_i \sqrt{\lambda}_i{}^3 d\sqrt{\lambda}_i\right)\left(\bigwedge_{c=1}^{3}\bigwedge_i \mathrm{d}V_{ii}^{(c)}\right)\left(\bigwedge_{c=0}^{3}\bigwedge_{i<j}\mathrm{d}U_{ij}^{(c)} \wedge \mathrm{d}V_{ij}^{(c)}(\lambda_i - \lambda_j)\right)\\ =& \ \mathrm{d}U_{\mathrm{Haar}}\mathrm{d}V_{\mathrm{Haar}}2^{-n}\bigwedge_i \mathrm{d}\lambda_i\,\lambda_i\Delta(\lambda)^4.\end{aligned} \tag{B3}$$

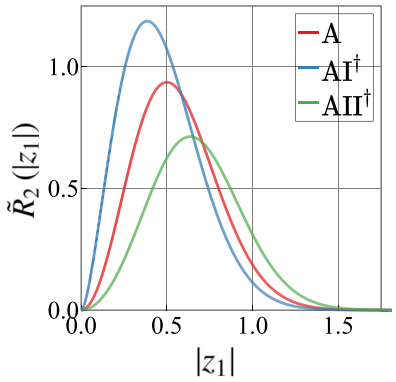

Figure 10. Two-point correlation functions $R_2(z_1, z_2)$ of 2×2 (4×4) non-Hermitian random matrices in classes A and AI† (AII†). The vertical axis $\tilde{R}_2(|z_1|)$ is defined by $R_2(z_1, z_2) =: \delta(z_1 + z_2)\,\tilde{R}_2(|z_1|)$. The normalization constants are chosen as $C_2 = C_3 = C_5 = 1$.

Appendix C. Two-point correlation functions of small non-Hermitian random matrices

In this appendix, we calculate the two-point correlation function of 2×2 (4×4) non-Hermitian random matrices in classes A and AI† (class AII†). Similar to the Wigner surmise, this gives a simple analytical expression for the two-point function. We should however keep in mind that the small-N result may not be a good approximation to the large-N limit. See similar comments around equation (25).

In these cases, non-Hermitian random matrices host only an opposite-sign pair of complex eigenvalues. The two-point correlation function reads

$$R_2(z_1, z_2) = \delta(z_1 + z_2)\,\langle \mathrm{tr}\,\delta(z_1 - H)\rangle. \tag{C1}$$

Here, $\langle \mathrm{tr}\,\delta(z_1 - z)\rangle$ depends only on $|z_1|$ and is given as $2\langle\delta(z_1 - z)\rangle$ with an eigenvalue $z\in\mathbb{C}$ of H. Hence, we have

$$R_2(z_1, z_2) = \frac{\delta(z_1 + z_2)\,\langle\delta(|z_1| - |z|)\rangle}{\pi\,|z_1|}. \tag{C2}$$

On the other hand, the level-spacing distributions are defined as

$$p_{\mathrm{s}}(s) := \langle\delta(s - 2|z|)\rangle. \tag{C3}$$

Consequently, we have (figure 10)

$$\begin{aligned} R_2(z_1, z_2) &= \frac{2\delta(z_1 + z_2)\,p_{\mathrm{s}}(2|z_1|)}{\pi\,|z_1|} \\ &= \frac{2}{\pi}\delta(z_1 + z_2)\begin{cases} 16C_2^4|z_1|^2 K_0\left(4C_2^2|z_1|^2\right) & (\text{class AI}^\dagger); \\ 16C_3^4|z_1|^2 e^{-4C_3^2|z_1|^2} & (\text{class A}); \\ \left(16C_5^4|z_1|^2/3\right)\left(1 + 4C_5^2|z_1|^2\right)\mathrm{e}^{-4C_5^2|z_1|^2} & (\text{class AII}^\dagger), \end{cases} \end{aligned} \tag{C4}$$

with the modified Bessel function of the second kind, $K_0(x)$. Here, we use the analytical results of $p_s(s)$ in [48] with arbitrary positive constants C_2, C_3, $C_5 \geqslant 0$. For $|z_1|$, $|z_2| \ll 1$, we have

$$R_2(z_1, z_2) \simeq \frac{2}{\pi}\delta(z_1 + z_2) \begin{cases} -16C_2^4 |z_1|^2 \ln\left(4C_2^2 |z_1|^2\right) & \left(\text{class AI}^\dagger\right); \\ 16C_3^4 |z_1|^2 & \left(\text{class A}\right); \\ 16C_5^4 |z_1|^2/3 & \left(\text{class AII}^\dagger\right). \end{cases} \tag{C5}$$

ORCID iDs

Anish Kulkarni https://orcid.org/0000-0002-8477-7137
Shinsei Ryu https://orcid.org/0000-0002-1494-1253

References

[1] Wigner E P 1951 On the statistical distribution of the widths and spacings of nuclear resonance levels *Math. Proc. Cambridge Philos. Soc.* **47** 790
[2] Wigner E P 1958 On the distribution of the roots of certain symmetric matrices *Ann. Math.* **67** 325
[3] Akemann G, Baik J and Di Francesco P 2015 *The Oxford Handbook of Random Matrix Theory* (*Oxford Handbooks in Mathematics*) (Oxford University Press)
[4] Byun S-S and Forrester P J 2024 *Progress on the Study of the Ginibre Ensembles* (Springer)
[5] Konotop V V, Yang J and Zezyulin D A 2016 Nonlinear waves in $\mathcal{PT}$-symmetric systems *Rev. Mod. Phys.* **88** 035002
[6] El-Ganainy R, Makris K G, Khajavikhan M, Musslimani Z H, Rotter S and Christodoulides D N 2018 Non-Hermitian physics and PT symmetry *Nat. Phys.* **14** 11
[7] Ginibre J 1965 Statistical ensembles of complex, quaternion and real matrices *J. Math. Phys.* **6** 440
[8] Girko V L 1985 Circular law *Theory Probab. Appl.* **29** 694
[9] Verbaarschot J J M, Weidenmüller H A and Zirnbauer M R 1985 Grassmann integration in stochastic quantum physics: the case of compound-nucleus scattering *Phys. Rep.* **129** 367
[10] Sokolov V V and Zelevinsky V G 1988 On a statistical theory of overlapping resonances *Phys. Lett.* B **202** 10
[11] Sokolov V V and Zelevinsky V G 1989 Dynamics and statistics of unstable quantum states *Nucl. Phys.* A **504** 562
[12] Haake F, Izrailev F, Lehmann N, Saher D and Sommers H-J 1992 Statistics of complex levels of random matrices for decaying systems *Z. Phys.* B **88** 359
[13] Stephanov M A 1996 Random matrix model of QCD at finite density and the nature of the quenched limit *Phys. Rev. Lett.* **76** 4472
[14] Fyodorov Y V, Khoruzhenko B A and Sommers H-J 1997 Almost-Hermitian random matrices: eigenvalue density in the complex plane *Phys. Lett.* A **226** 46
[15] Kogut J B, Stephanov M A, Toublan D, Verbaarschot J J M and Zhitnitsky A 2000 QCD-like theories at finite baryon density *Nucl. Phys.* B **582** 477
[16] Hatano N and Nelson D R 1996 Localization transitions in non-hermitian quantum mechanics *Phys. Rev. Lett.* **77** 570
[17] Efetov K B 1997 Directed quantum chaos *Phys. Rev. Lett.* **79** 491
[18] Feinberg J and Zee A 1997 Non-hermitian random matrix theory: method of hermitian reduction *Nucl. Phys.* B **504** 579
[19] Efetov K B 1997 Quantum disordered systems with a direction *Phys. Rev.* B **56** 9630
[20] Hatano N and Nelson D R 1997 Vortex pinning and non-Hermitian quantum mechanics *Phys. Rev.* B **56** 8651
[21] Brouwer P W, Silvestrov P G and Beenakker C W J 1997 Theory of directed localization in one dimension *Phys. Rev.* B **56** R4333(R)
[22] Feinberg J and Zee A 1999 Non-Hermitian localization and delocalization *Phys. Rev.* E **59** 6433
[23] Longhi S 2019 Topological phase transition in non-Hermitian quasicrystals *Phys. Rev. Lett.* **122** 237601
[24] Zeng Q-B, Yang Y-B and Xu Y 2020 Topological phases in non-Hermitian Aubry-André-Harper models *Phys. Rev.* B **101** 020201

[25] Tzortzakakis A F, Makris K G and Economou E N 2020 Non-Hermitian disorder in two-dimensional optical lattices *Phys. Rev.* B **101** 014202
[26] Huang Y and Shklovskii B I 2020 Anderson transition in three-dimensional systems with non-Hermitian disorder *Phys. Rev.* B **101** 014204
[27] Kawabata K and Ryu S 2021 Nonunitary scaling theory of Non-Hermitian localization *Phys. Rev. Lett.* **126** 166801
[28] Claes J and Hughes T L 2021 Skin effect and winding number in disordered non-Hermitian systems *Phys. Rev.* B **103** L140201
[29] Luo X, Ohtsuki T and Shindou R 2021 Universality classes of the Anderson transitions driven by Non-Hermitian disorder *Phys. Rev. Lett.* **126** 090402
[30] Luo X, Ohtsuki T and Shindou R 2021 Transfer matrix study of the Anderson transition in non-Hermitian systems *Phys. Rev.* B **104** 104203
[31] Luo X, Xiao Z, Kawabata K, Ohtsuki T and Shindou R 2022 Unifying the Anderson transitions in Hermitian and non-Hermitian systems *Phys. Rev. Res.* **4** L022035
[32] Liu H, You J-S, Ryu S and Fulga I C 2021 Supermetal-insulator transition in a non-Hermitian network model *Phys. Rev.* B **104** 155412
[33] Bergholtz E J, Budich J C and Kunst F K 2021 Exceptional topology of non-Hermitian systems *Rev. Mod. Phys.* **93** 015005
[34] Okuma N and Sato M 2023 Non-Hermitian topological phenomena: a review *Annu. Rev. Condens. Matter Phys.* **14** 83
[35] Altland A and Zirnbauer M R 1997 Nonstandard symmetry classes in mesoscopic normal-superconducting hybrid structures *Phys. Rev.* B **55** 1142
[36] Evers F and Mirlin A D 2008 Anderson transitions *Rev. Mod. Phys.* **80** 1355
[37] Chiu C-K, Teo J C Y, Schnyder A P and Ryu S 2016 Classification of topological quantum matter with symmetries *Rev. Mod. Phys.* **88** 035005
[38] Haake F, Gnutzmann S and Kuś M 2018 *Quantum Signatures of Chaos* (Springer)
[39] Bernard D and LeClair A 2002 A classification of Non-Hermitian random matrices *Statistical Field Theories* ed A Cappelli and G Mussardo (Springer) pp 207–14
[40] Kawabata K, Shiozaki K, Ueda M and Sato M 2019 Symmetry and topology in Non-Hermitian physics *Phys. Rev.* X **9** 041015
[41] Grobe R, Haake F and Sommers H-J 1988 Quantum distinction of regular and chaotic dissipative motion *Phys. Rev. Lett.* **61** 1899
[42] Grobe R and Haake F 1989 Universality of cubic-level repulsion for dissipative quantum chaos *Phys. Rev. Lett.* **62** 2893
[43] Xu Z, García-Pintos L P, Chenu A and del Campo A 2019 Extreme decoherence and quantum chaos *Phys. Rev. Lett.* **122** 014103
[44] Hamazaki R, Kawabata K and Ueda M 2019 Non-Hermitian many-body localization *Phys. Rev. Lett.* **123** 090603
[45] Denisov S, Laptyeva T, Tarnowski W, Chruściński D and Życzkowski K 2019 universal spectra of random lindblad operators *Phys. Rev. Lett.* **123** 140403
[46] Can T, Oganesyan V, Orgad D and Gopalakrishnan S 2019 Spectral gaps and midgap states in random quantum master equations *Phys. Rev. Lett.* **123** 234103
[47] Can T 2019 Random Lindblad dynamics *J. Phys. A: Math. Theor.* **52** 485302
[48] Hamazaki R, Kawabata K, Kura N and Ueda M 2020 Universality classes of non-Hermitian random matrices *Phys. Rev. Res.* **2** 023286
[49] Akemann G, Kieburg M, Mielke A and Prosen T 2019 universal signature from integrability to chaos in dissipative open quantum systems *Phys. Rev. Lett.* **123** 254101
[50] Sá L, Ribeiro P and Prosen T 2020 Complex spacing ratios: a signature of dissipative quantum chaos *Phys. Rev.* X **10** 021019
[51] Wang K, Piazza F and Luitz D J 2020 Hierarchy of relaxation timescales in local random Liouvillians *Phys. Rev. Lett.* **124** 100604
[52] Xu Z, Chenu A, Prosen T and del Campo A 2021 Thermofield dynamics: quantum chaos versus decoherence *Phys. Rev.* B **103** 064309
[53] García-García A M, Jia Y, Rosa D and Verbaarschot J J M 2022 Dominance of replica off-diagonal configurations and phase transitions in a *PT* symmetric Sachdev-Ye-Kitaev model *Phys. Rev. Lett.* **128** 081601
[54] Li J, Prosen T and Chan A 2021 Spectral statistics of non-Hermitian matrices and dissipative quantum chaos *Phys. Rev. Lett.* **127** 170602

[55] Cornelius J, Xu Z, Saxena A, Chenu A and del Campo A 2022 Spectral filtering induced by non-Hermitian evolution with balanced gain and loss: enhancing quantum chaos *Phys. Rev. Lett.* **128** 190402
[56] García-García A M, Sá L and Verbaarschot J J M 2022 Symmetry classification and universality in non-Hermitian many-body quantum chaos by the Sachdev-Ye-Kitaev model *Phys. Rev.* X **12** 021040
[57] Prasad M, Yadalam H K, Aron C and Kulkarni M 2022 Dissipative quantum dynamics, phase transitions and non-Hermitian random matrices *Phys. Rev.* A **105** L050201
[58] Sá L, Ribeiro P and Prosen T 2022 Lindbladian dissipation of strongly-correlated quantum matter *Phys. Rev. Res.* **4** L022068
[59] Kulkarni A, Numasawa T and Ryu S 2022 Lindbladian dynamics of the Sachdev-Ye-Kitaev model *Phys. Rev.* B **106** 075138
[60] García-García A M, Jia Y, Rosa D and Verbaarschot J J M 2022 Replica symmetry breaking in random non-Hermitian systems *Phys. Rev.* D **105** 126027
[61] Cipolloni G and Kudler-Flam J 2023 Entanglement entropy of Non-Hermitian eigenstates and the Ginibre ensemble *Phys. Rev. Lett.* **130** 010401
[62] Xiao Z, Kawabata K, Luo X, Ohtsuki T and Shindou R 2022 Level statistics of real eigenvalues in non-Hermitian systems *Phys. Rev. Res.* **4** 043196
[63] Shivam S, De Luca A, Huse D A and Chan A 2023 Many-body quantum chaos and emergence of Ginibre ensemble *Phys. Rev. Lett.* **130** 140403
[64] Ghosh S, Gupta S and Kulkarni M 2022 Spectral properties of disordered interacting non-Hermitian systems *Phys. Rev.* B **106** 134202
[65] Sá L, Ribeiro P and Prosen T 2023 Symmetry classification of many-body Lindbladians: tenfold way and beyond *Phys. Rev.* X **13** 031019
[66] Kawabata K, Kulkarni A, Li J, Numasawa T and Ryu S 2023 Symmetry of open quantum systems: classification of dissipative quantum chaos *PRX Quantum* **4** 030328
[67] Cipolloni G and Kudler-Flam J 2024 Non-Hermitian Hamiltonians violate the eigenstate thermalization hypothesis *Phys. Rev.* B **109** L020201
[68] Kawabata K, Xiao Z, Ohtsuki T and Shindou R 2023 Singular-value statistics of non-Hermitian random matrices and open quantum systems *PRX Quantum* **4** 040312
[69] Xiao Z, Shindou R and Kawabata K 2024 Universal hard-edge statistics of non-Hermitian random matrices *Phys. Rev. Res.* **6** 023303
[70] Efetov K 1996 *Supersymmetry in Disorder and Chaos* (Cambridge University Press)
[71] Nishigaki S M and Kamenev A 2002 Replica treatment of non-Hermitian disordered Hamiltonians *J. Phys. A: Math. Gen.* **35** 4571
[72] Kamenev A and Mézard M 1999 Wigner-Dyson statistics from the replica method *J. Phys. A: Math. Gen.* **32** 4373
[73] Kamenev A and Mézard M 1999 Level correlations in disordered metals: the replica σ model *Phys. Rev.* B **60** 3944
[74] Yurkevich I V and Lerner I V 1999 Nonperturbative results for level correlations from the replica nonlinear σ model *Phys. Rev.* B **60** 3955
[75] Mehta M L 2004 *Random Matrices* (Elsevier)
[76] Chen Z, Kawabata K, Kulkarni A and Ryu S 2025 Field theory of non-Hermitian disordered systems *Phys. Rev.* B **111** 054203
[77] Nishigaki S 2016 *Random Matrices and Gauge Theory* (Saiensu-Sha) (www.saiensu.co.jp/search/?isbn=978-4-7819-9015-6&y=2024#detail)
[78] Akemann G, Aygün N, Kieburg M, and Päßler P 2024 Complex symmetric, self-dual, and Ginibre random matrices: analytical results for three classes of bulk and edge statistics (arXiv:2410.21032)
[79] Forrester P J 2024 Dualities for characteristic polynomial averages of complex symmetric and self dual non-Hermitian random matrices (arXiv:2411.07356)
[80] Liu D-Z and Zhang L 2024 Duality in non-Hermitian random matrix theory *Nucl. Phys.* B **1004** 116559
[81] Akemann G, Mielke A and Päßler P 2022 Spacing distribution in the two-dimensional Coulomb gas: Surmise and symmetry classes of non-Hermitian random matrices at noninteger β *Phys. Rev.* E **106** 014146
[82] Verbaarschot J J M and Zirnbauer M R 1985 Critique of the replica trick *J. Phys. A: Math. Gen.* **18** 1093

[83] Zirnbauer M R 1999 Another critique of the replica trick (arXiv:cond-mat/9903338)
[84] Kanzieper E 2002 Replica field theories, Painlevé transcendents and exact correlation functions *Phys. Rev. Lett.* **89** 250201
[85] Splittorff K and Verbaarschot J J M 2003 Replica limit of the Toda lattice equation *Phys. Rev. Lett.* **90** 041601
[86] Kanzieper E 2005 Exact replica treatment of non-Hermitean complex random matrices (arXiv:cond-mat/0312006)
[87] Edelman A and Jeong S 2023 Fifty three matrix factorizations: a systematic approach *SIAM J. Matrix Anal. Appl.* **44** 415
[88] Liu Y, Kudler-Flam J and Kawabata K 2023 Symmetry classification of typical quantum entanglement *Phys. Rev.* B **108** 085109
[89] Kulkarni A K Internal symmetry and dynamical phenomena in open quantum systems (Non-Hermitian topology, geometry and symmetry across physical platforms, October 7th, 2024)